

Review

# Magnetite (Fe<sub>3</sub>O<sub>4</sub>) Nanoparticles in Biomedical Application: From Synthesis to Surface Functionalisation

Lokesh Srinath Ganapathe <sup>1</sup>, Mohd Ambri Mohamed <sup>1</sup> , Rozan Mohamad Yunus <sup>2</sup>  and Dilla Duryha Berhanuddin <sup>1,\*</sup>

<sup>1</sup> Institut Kejuruteraan Mikro dan Nanoelektronik (IMEN), Universiti Kebangsaan Malaysia, Bangi 43600, Selangor Darul Ehsan, Malaysia; p99857@siswa.ukm.edu.my (L.S.G.); ambri@ukm.edu.my (M.A.M.)

<sup>2</sup> Fuel Cell Institute, Level 4, Research Complex, Universiti Kebangsaan Malaysia, Bangi 43600, Selangor, Malaysia; rozanyunus@ukm.edu.my

\* Correspondence: dduryha@ukm.edu.my; Tel.: +60-38911-8544

Received: 28 October 2020; Accepted: 20 November 2020; Published: 3 December 2020



**Abstract:** Nanotechnology has gained much attention for its potential application in medical science. Iron oxide nanoparticles have demonstrated a promising effect in various biomedical applications. In particular, magnetite (Fe<sub>3</sub>O<sub>4</sub>) nanoparticles are widely applied due to their biocompatibility, high magnetic susceptibility, chemical stability, innocuousness, high saturation magnetisation, and inexpensiveness. Magnetite (Fe<sub>3</sub>O<sub>4</sub>) exhibits superparamagnetism as its size shrinks in the single-domain region to around 20 nm, which is an essential property for use in biomedical applications. In this review, the application of magnetite nanoparticles (MNPs) in the biomedical field based on different synthesis approaches and various surface functionalisation materials was discussed. Firstly, a brief introduction on the MNP properties, such as physical, thermal, magnetic, and optical properties, is provided. Considering that the surface chemistry of MNPs plays an important role in the practical implementation of in vitro and in vivo applications, this review then focuses on several predominant synthesis methods and variations in the synthesis parameters of MNPs. The encapsulation of MNPs with organic and inorganic materials is also discussed. Finally, the most common in vivo and in vitro applications in the biomedical world are elucidated. This review aims to deliver concise information to new researchers in this field, guide them in selecting appropriate synthesis techniques for MNPs, and to enhance the surface chemistry of MNPs for their interests.

**Keywords:** magnetite; Fe<sub>3</sub>O<sub>4</sub>; magnetite nanoparticles; biomedical application

## 1. Introduction

Nanotechnology has become one of the utmost essentials for the sophistication of science because it utilises matter manipulation on a scale where materials portray different and appealing characteristics compared with others in the micro-macro scale. It has attracted much attention, particularly that of medical research, which hugely affects the global economy. Nanoparticles are particles with sizes ranging between 1 and 1000 nm [1,2]. They are often used in the biomedical field due to their superior nature over sheer-sized particles, e.g., larger surface-to-volume ratio, high magnetic characteristics, high activity, and novel optical properties. Nanoparticles possess a high applicability amongst cells and biomolecules. This interaction is influenced by the agglomeration, charge, chemical composition, crystalline structure, shape, size, and solubility of nanoparticles [3–5].

Amongst them, magnetic nanoparticles are substantially utilised in bioanalytical techniques and biomedical applications. They encounter less background interference with bio-type specimens, making the magnetic susceptibilities of biotype samples nearly trivial. Given this advantage, biological samples are easily accessible towards the external magnetic field [6,7]. Nowadays, magnetic nanoparticles have

the capability of design integration for a huge range of biomedical applications, such as analytical tools, bioimaging, biosensors, contrast agents (CAs), hyperthermia, photoablation therapy, physical therapy applications, separation, signal markers, and targeted drug delivery (TDD) [1–8].

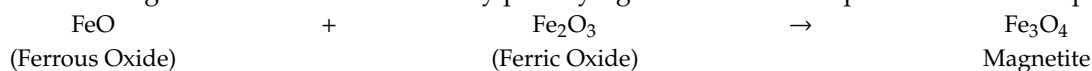
Iron oxide nanoparticles (IONPs) were used in most studies due to their biocompatibility, high saturation magnetisation, high magnetic susceptibility, chemical stability, and innocuousness. IONPs with high magnetic properties, including nickel and cobalt, easily oxidise and are toxic. Magnetite ( $\text{Fe}_3\text{O}_4$ ) nanoparticles (MNPs) are by far the most employed IONPs in biomedical applications [4]. Magnetite nanoparticles demonstrate distinctive electrical and magnetic characteristics as a result of the transfer of ions from  $\text{Fe}^{2+}$  ions to  $\text{Fe}^{3+}$  ions. The MNPs used in the biomedical field are normally smaller than 20 nm, thereby displaying superparamagnetism properties. They are also highly utilised in this field compared with other magnetic-IONPs (M-IONPs) due to their biocompatible surface chemistry, high magnetisation saturation value, narrowed particle size distribution (<100 nm), and superparamagnetism property [8–10].

The utilisation of MNPs in the biomedical field is specifically discussed in the present paper. The general properties of MNPs are first presented, followed by the synthesis techniques and surface functionalisation of MNPs. Finally, the MNP applications, which were segregated into in vivo and in vitro applications, in the biomedical field are discussed.

## 2. Properties of Magnetite ( $\text{Fe}_3\text{O}_4$ ) Nanoparticles

Among the M-IONPs family, the three most popular M-IONPs are magnetite ( $\text{Fe}_3\text{O}_4$ ), maghemite ( $\gamma\text{-Fe}_2\text{O}_3$ ), and hematite ( $\alpha\text{-Fe}_2\text{O}_3$ ). In terms of chemical properties, hematite ( $\alpha\text{-Fe}_2\text{O}_3$ ) is the most stable compound in the presence of air for a long period of time. However, hematite ( $\alpha\text{-Fe}_2\text{O}_3$ ) has the weakest magnetic strength of the two mentioned M-IONPs. Maghemite ( $\gamma\text{-Fe}_2\text{O}_3$ ) is a phase that is formed upon the oxidation of magnetite ( $\text{Fe}_3\text{O}_4$ ) [2,4,11].

The term ‘magnetite’ is derived from the word ‘Magnesia’, which is a district in Asia Minor, where huge amounts of magnetite were discovered. Magnetite is also often deduced as iron (III) oxide due to its possession of ferric (oxidised) and ferrous (reduced) iron elements [12]. A typical synthesis reaction of magnetite is illustrated below by portraying the chemical composition of the compound:



Magnetite varies depending on the type of iron oxides, whether trivalent or divalent. The magnetite stoichiometric of  $\text{Fe}^{2+}:\text{Fe}^{3+}$  is 1:2, where divalent irons could be completely or partially substituted by Zn, Mn, Co and other divalent ions. Thus, magnetite could behave as an n-type or a p-type semiconductor [13].

### 2.1. Structural and Physical

The electronic configuration of  $\text{Fe}^{2+}$  ion is  $[\text{Ar}] 3d^6$ , while that of  $\text{Fe}^{3+}$  ion is  $[\text{Ar}] 3d^5$ . In both scenarios, the 3d electron orbital is the one that governs specific properties of the Fe atom. Magnetite has a crystalline structure, which is a cubic inverse spinel structure packed along the [1, 1, 1] plane, in which  $\text{Fe}^{2+}$  and  $\text{Fe}^{3+}$  occupy the octahedral lattice voids and  $\text{Fe}^{3+}$  occupies the tetrahedral lattice voids [10,14], as illustrated in Figure 1. The formula can be denoted as  $\text{Fe}^{3+}(\text{A})[\text{Fe}^{2+}\text{Fe}^{3+}](\text{B})\text{O}_4$ , where A is tetrahedral and B is octahedral [15,16]. Brisk electrons hopping on the octahedral sites between the  $\text{Fe}^{2+}$  and  $\text{Fe}^{3+}$  ions could stimulate the conductivity of magnetite [17].

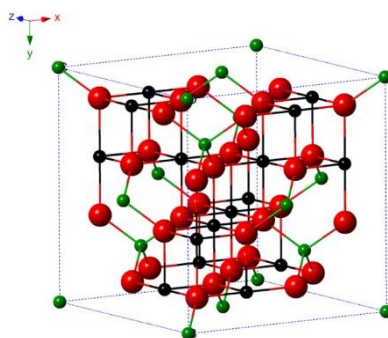


**Figure 1.** Crystal structure of magnetite ( $\text{Fe}_3\text{O}_4$ ). The green balls are ferric ions; the red balls are oxygen ions; and the black balls are ferrous ions [13]. [Reprinted with permission from Wu et al. [13]. Published 2015 by Taylor and Francis under the Creative Commons Attribution 3.0 (CC-BY-3.0) License].

As observed in Figure 1, magnetite possesses a face-centred cubic spinel unit cell with a unit length of  $\alpha = 0.839$  nm. This cell consists of 32  $\text{O}^{2-}$  ions and a [1, 1, 1] compact alignment [13,18]. As for the physical properties of magnetite ( $\text{Fe}_3\text{O}_4$ ), the pure magnetite in powder form and the colloidal magnetite solutions are archetypally distinguished by jet-black colour [12]. Upon exposure to air (oxidation), magnetite ( $\text{Fe}_3\text{O}_4$ ) oxidises to maghemite ( $\gamma\text{-Fe}_2\text{O}_3$ ), which is quintessentially denoted in brownish colour. The annealing process of maghemite ( $\gamma\text{-Fe}_2\text{O}_3$ ) at approximately 700 °C transforms maghemite ( $\gamma\text{-Fe}_2\text{O}_3$ ) into hematite ( $\alpha\text{-Fe}_2\text{O}_3$ ), which has a reddish tone.

## 2.2. Thermal

Magnetite comes from the Spinel mineral family. It mostly possesses different kinetic-based characteristics: the behaviour of MNPs differ at three different phases of temperature. The first phase is the Verwey temperature, where the Verwey transition ranges between 0 K and 119 K. At this phase, magnetite converts from semiconductor to metal phase [19]. The second phase is the Curie temperature ( $T_C$ ), ranging between 120 K and 840 K (to be discussed further in Section 2.3). The third phase is when the temperature is above 840 K, where MNPs behave as a paramagnetic metal [20].

In terms of electrical conductivity, a significant decline in temperature at around 120 K of the order of 90 times caused the MNPs to convert from cubic structure to orthorhombic structure, which is a lower ordering of symmetry [20,21]. The thermal properties of MNPs are highly important in the biomedical field, especially for the usage of MNPs as thermal seeds in magnetic hyperthermia therapy (MHT).

Two distinct curves can be obtained from the magnetization-temperature (M-T) measurement of MNPs known as zero field cooling (ZFC) and field cooling (FC). In ZFC, the magnetic moment increased with the temperature and then decreased, while the moment decreased in FC curve. The temperature at the peak point of ZFC value is the blocking temperature. As single domain structure, superparamagnetic MNPs can fluctuate randomly by thermal fluctuation at high temperatures. At low temperatures, the thermal energy becomes smaller and magnetic moments become blocked. It is at this temperature, and the magnetic moment becomes null. Below this temperature, superparamagnetic MNPs immobilise in the absence of a magnetic field ( $H$ ) [4].  $T_B$  varies between blocked state and superparamagnetic behaviour when  $H$  is changed; it possesses an inversely proportional relationship with  $H$  [22].

$T_B$  (i.e., energy barrier) is mostly measured using a superconducting quantum interference device (SQUID) from low field-cooled (FC) and zero FC magnetisation curves. Saragi et al. recently reported that the  $T_B$  of MNPs is 118.38 K at 100 Oe. A gradual increase in  $T_B$  with surface functionalisation was also previously reported [23].

For the application of MNPs in biomedicine, they should emit zero magnetic remanence in the absence of an external magnetic field, that is, they have to emit superparamagnetism properties. This is a phenomenon that occurs only below  $T_B$ . Therefore,  $T_B$  values have to be below room temperature to increase the potential of MNPs to be applied in the biomedical field [24]. In other words, at low  $T_B$ ,

superparamagnetic property of MNPs tend to prosper, which leads to a more efficient localized TDD, better contrast agent (CA) for MRI, and higher heat dissipation in MHT.

### 2.3. Magnetic

M-IONPs, especially hematite ( $\alpha\text{-Fe}_2\text{O}_3$ ) and maghemite ( $\gamma\text{-Fe}_2\text{O}_3$ ), possess the most robust magnetism among other transition metal oxides [25]. At the nanoscale level, magnetite ( $\text{Fe}_3\text{O}_4$ ) has shown ferrimagnetism characteristics, which bulk magnetite does not have [12]. This property is generated by the spin magnetic moments of  $\text{Fe}^{2+}$  and  $\text{Fe}^{3+}$  ions. These moments are aligned in a parallel position in the octahedral site. However, in the tetrahedral site, ferric ions are distributed in anti-parallel alignment. These phenomena naturally lead to the annihilation of the spin moments of all the ferric ions that do not stimulate  $\text{Fe}_3\text{O}_4$  net magnetisation, as illustrated in Table 1. By contrast, the ferrous ions have magnetic moments that are orientated in a uniformly aligned direction, with the entire moments bestowed for  $\text{Fe}_3\text{O}_4$  net magnetisation. Therefore, the saturation magnetisation of  $\text{Fe}_3\text{O}_4$  complies to the spike-up between each spin magnetic moment of the ferrous ions and their quantity. It is also related to the total naturally aligned ferrous ions in  $\text{Fe}_3\text{O}_4$ . The ferrimagnetism property of  $\text{Fe}_3\text{O}_4$  is generated by the parallel-aligned magnetic moments in tetrahedral positions and the unparallel alignment of  $\text{Fe}^{2+}$  and  $\text{Fe}^{3+}$  ion spins in octahedral positions [12,26].

**Table 1.** Spin magnetic moment distribution of  $\text{Fe}^{3+}$  and  $\text{Fe}^{2+}$  ions in  $\text{Fe}_3\text{O}_4$  elemental cell [26].

Cation	Octahedral Site	Tetrahedral Site	Net Magnetic Moment
Ferric ions	↑↑↑↑ ↑↑↑↑	↓↓↓↓ ↓↓↓↓	Complete annihilation
Ferrous ions	↑↑↑↑ ↑↑↑↑	-	↑↑↑↑

Any ferrimagnetic material (in this case, magnetite) normally possesses retentivity and coercivity, as shown in Figure 2 [27]. The reduction in particle size from bulk to nanoscale reduces the quantity of exchange-coupled spins that rebels magnetic reorientation spontaneously. This phenomenon results in superparamagnetic behaviour [12]. Further reduction in magnetite size leads to the exhibition of superparamagnetic characteristics. Moreover, an increase in temperature increases the particle's thermal energy, thus expediting the reorientation of magnetism, i.e., superparamagnetic magnetisation [12].

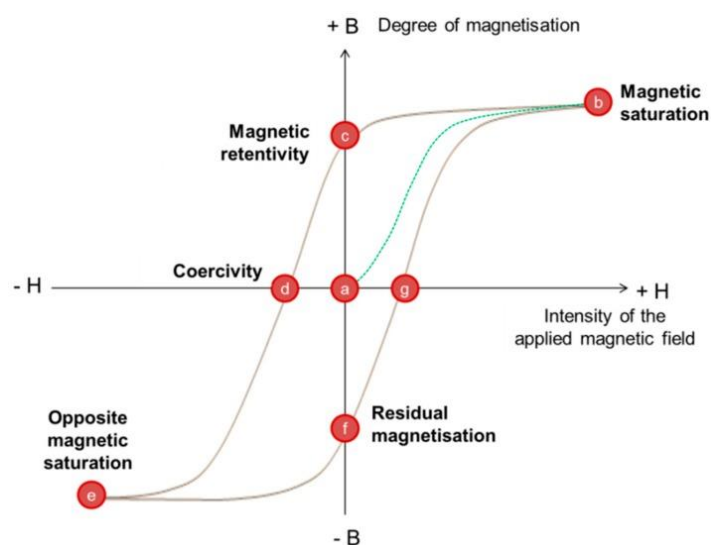


**Figure 2.** Hysteresis loop of a typical ferrimagnetism [27].

$T_C$  is defined as the temperature that occurs during the conversion of magnetisation from ferrimagnetic to superparamagnetic at a critical temperature. MNPs possess a high  $T_C$  at  $\sim 858$  K [10]. The high surface spin proportion raises the dipolar anisotropy, which consequently lowers down  $T_C$ . This temperature is where dipolar anisotropy and single ion are at an equilibrium state [12].

Thapa et al. showed that the concentration level of oxygen reduces as magnetite reaches the nanoscale, which causes a mild curtailment in the valence states of iron [28]. This event yields an increased content of  $\text{Fe}^{2+}$  ions as the magnetic moment is mainly subjected to the ferrous species. In chemistry, the reduction in oxygen is termed as reduction process. A further reduction in magnetite results in increased magnetic strength, which means increased saturation magnetisation values [29,30].

Saturation magnetization is a point at which a particular material cannot be magnetized further with applied magnetic field. In a simple term, saturation magnetization value displays the magnetic strength of a particular material. At room temperature, MNPs show ferrimagnetism, where the saturation magnetisation value at a magnetic field of 1.5 T is up to  $88.1 \text{ emu g}^{-1}$  [31]. The high saturation magnetization value of MNPs constitute one of the most important properties in terms of biomedical application. It helps in drug delivery to cancer cells through an external magnetic field and acts as a good contrast agent (CA) for high-resolution image projection in magnetic resonance imaging (MRI).

#### 2.4. Optical

Magnetite is continuously studied extensively in the field of optics. Optical research on magnetite was carried out through polarisation [32], photoelectron, magneto-optical spectroscopy [33,34], and reflectivity [14,35] approaches. This research is important in biomedical applications because the optical properties of magnetite could be further altered to be used in bioimaging and light-based hyperthermia therapy.

##### 2.4.1. Electronic Band Structure

Research has shown that the valence band of oxygen ( $2p$ ) to the void iron ( $4s$ ) is apart by  $\sim 4\text{--}6$  eV [36]. The tetrahedral and octahedral crystal field bands consist of 3d metal atomic orbitals existing in between the abovementioned range. Several theoretical calculations and experimental measurements have shown that the crystal field, which splits on the tetrahedral site, induces energy gap values ( $\Delta_{cf,t}$ ) of  $\sim 0.9$  and  $\sim 2.2$  eV for the octahedral site ( $\Delta_{cf,o}$ ). In addition,  $2p$  is further apart by a value of approximately  $\sim 0.9$  eV in the crystal field site  $t_{2g,e}$  of both sites [37,38].

Alvarado et al. have reported on the photoelectron and polarisation of magnetite. In particular, the one-electron energy level of magnetite was investigated to elucidate 3d photoelectronic excitation [32]. Antonov et al. theoretically studied the magneto-optical Kerr effect and electronic structure of magnetite by utilising local spin density approximation (LSDA) and LSDA + U techniques [36]. LSDA is an approximation technique to determine the exchange–correlation energy functional in density functional theory, while LSDA + U is the charge ordering of energy-band structure. Both of these approximation techniques consist of complex computational approaches, which involve several divisions and sub-divisions. A more detailed discussion on this approximation technique can be found in this research paper [39]. Experimental magneto-optical and optical spectra of magnetite have illustrated a good agreement with the theoretical calculation from the LSDA + U approach. Figure 3 demonstrates the various inter-band transitions in relation to the absorptive section of the diagonal optical conductivity of magnetite: *A* represents the tetrahedral lattice sites; *B* is the octahedral lattice sites; *B1* and *B2* are the long-range charge ordering of ferric and ferrous ions; and finally others like  $a_{1g}$ ,  $t_{2g}$ , and  $e_g$  are all orbitals.

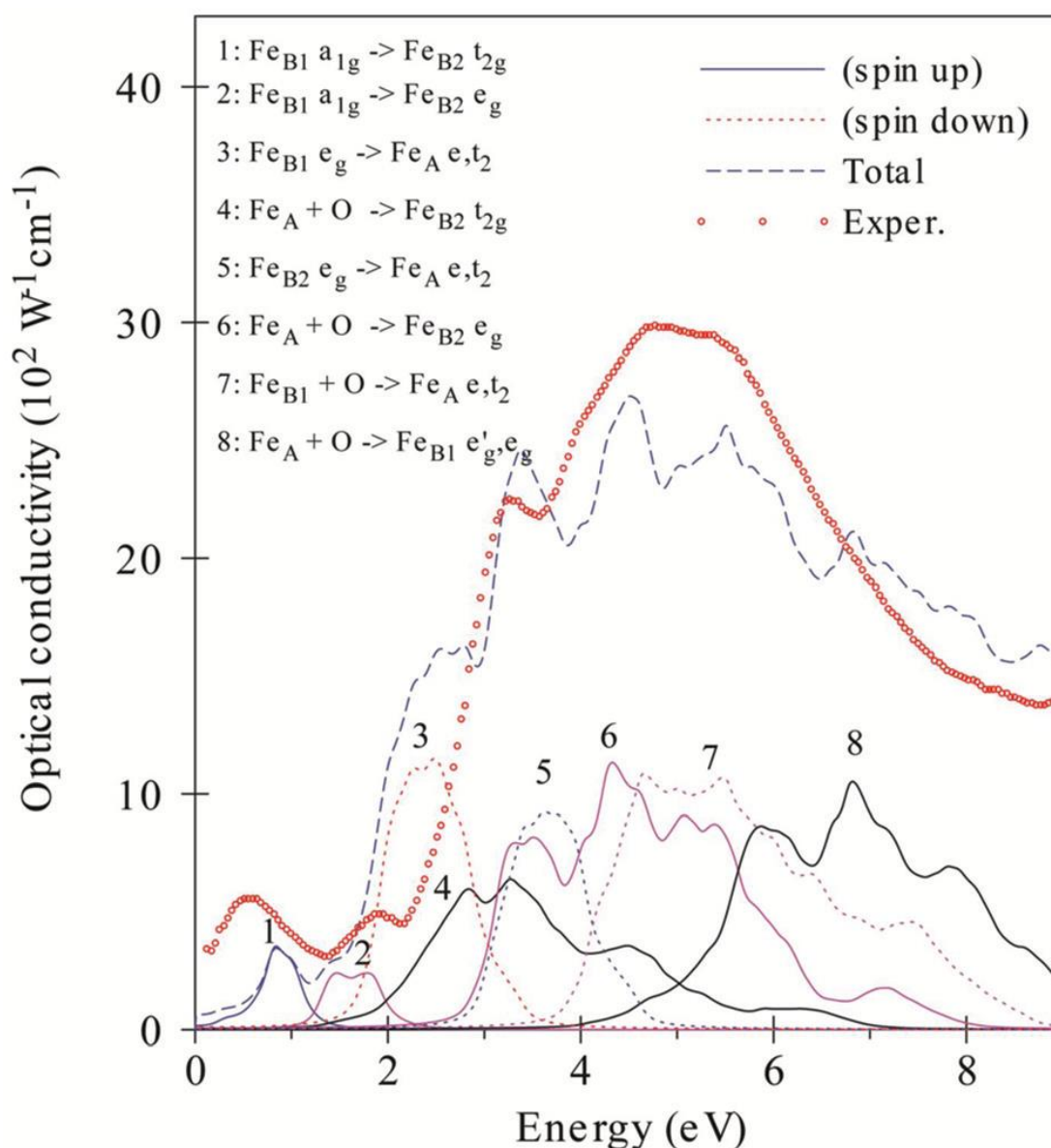


**Figure 3.** Various inter-band transitions in relation to the absorptive section of the diagonal optical conductivity of magnetite [39]. The circles depict experimental data reported by Park et al. [40]. [Reprinted with permission from Antonov et al. [39] and Park et al. [40]. Copyright 1998 and 2001 American Physical Society].

The first two peaks, 0.9 and 2 eV, were attributed to the  $\text{Fe}_{\text{B}}^{2+}(a_{1g}\uparrow) \rightarrow \text{Fe}_{\text{B}}^{3+}(t_{2g}\uparrow)$  and  $\text{Fe}_{\text{B}}^{2+}(a_{1g}\uparrow) \rightarrow \text{Fe}_{\text{B}}^{3+}(e_g\uparrow)$  inter-band transition, respectively. The third (2.2 eV) and the fifth (3.2 eV) peaks were attributed to the transition of  $\text{Fe}_{\text{B}}^{2+}(e_{g\downarrow}) \rightarrow \text{Fe}_{\text{A}}^{3+}(e_{\downarrow}t_{2\downarrow})$  and  $\text{Fe}_{\text{B}}^{3+}(e_{g\downarrow}) \rightarrow \text{Fe}_{\text{A}}^{3+}(e_{\downarrow}t_{2\downarrow})$ , respectively. The fourth, sixth, seventh and eighth peaks were due to the oxygen ( $2p$ ) to iron ( $3d$ ) transitions [34,38–40].

These findings provide insight regarding the band structure of MNPs, which can be applied in photothermal heating (light-based hyperthermia therapy) based on the photoluminescence characterization [41].

#### 2.4.2. Reflectivity of Magnetite

Few studies have reported on the reflectivity of magnetite and its applications. For instance, Schlegel et al. investigated the effect of conduction electrons and intra-band transition to the optical spectrum of magnetite [33]. They measured the reflectivity of magnetite by comparing the intensities

between the incident and reflected light beams in reference to the normal incidence over the whole photon energy range measured by utilising three spectrometers with ranges partially overlapping and a photon energy range that is fixed at 0.5–5 eV [14].

Figure 4 shows the reflectivity spectrum of Fe<sub>3</sub>O<sub>4</sub> at 300 K in the ultraviolet and visible energy ranges, where the spectral photon energy range was structured up until 5 eV.

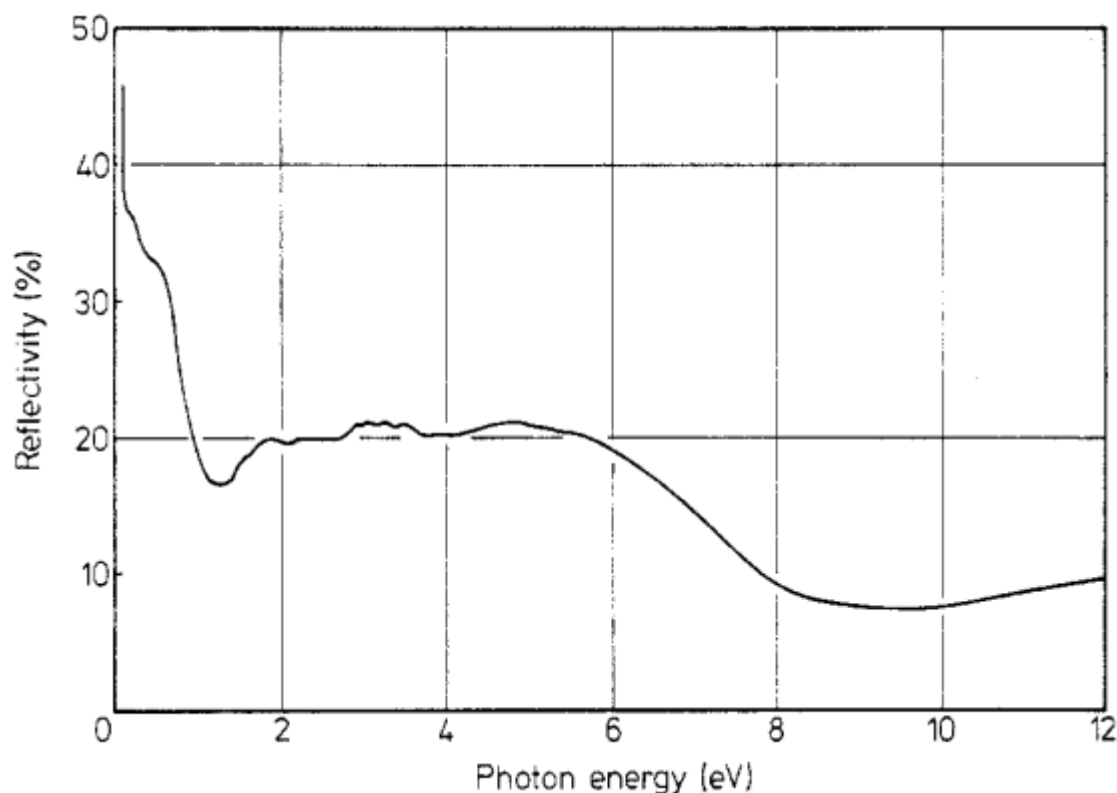


**Figure 4.** Reflectivity of Fe<sub>3</sub>O<sub>4</sub> at room temperature [14]. [Reflectivity of Fe<sub>3</sub>O<sub>4</sub> at room temperature. Reprinted with permission from Schlegel et al. [14] Copyright 1979 IOP 205 Publishing].

Compared with the reflectivity of magnetite in the infrared energy range at 300 K (Figure 5), the reflectivity at room temperature showed an increase, albeit at a much lower photon energy in the infrared spectral range. A slight decline in the reflectivity was also observed compared with that at 20 K. These results clearly prove that magnetite possesses a better reflectivity in the infrared energy region.

Figure 5 shows that the reflectivity in the infrared energy range was highly temperature-dependent [35]. Therefore, the high reflectivity values towards low photon energies at 300 K were caused by the intra-band transition of conduction electrons, whilst the decline in reflectivity values at Verwey transition temperature of 20 K gives magnetite more of semiconductor-like characteristics [14]. The optical properties of MNPs have been shown to display multimodal functionality applications in image-assisted diagnosis with MRI by projecting deep tissue imaging, and light-based hyperthermia therapy, which heats up solid tumours through near infrared radiation. These have proved the applicability and versatility of MNPs in clinical use.

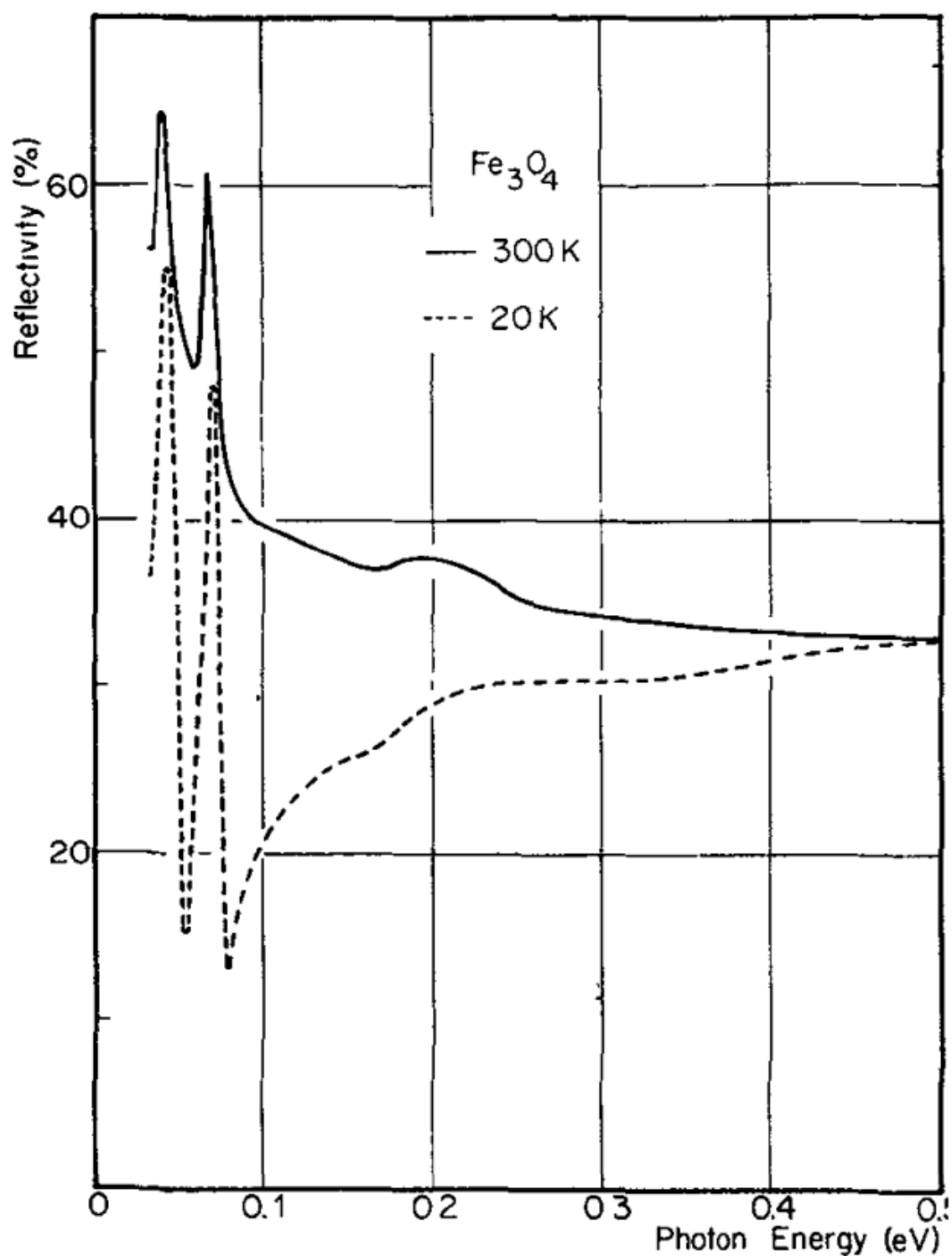


Figure 5. Reflectivity of Fe<sub>3</sub>O<sub>4</sub> in the infrared energy range [35].

### 2.5. Summary

A summary of the properties of MNPs is shown in Table 2. Amongst them, the most important feature in the biological field is the saturation magnetisation values. High saturation magnetisation values result in eased drug delivery to cancer cells, increased resolution of image projection in MRI, and improved heat dissipation in MHT.

**Table 2.** Summary of the properties of magnetite nanoparticles [42–44].

Properties	Magnetite Nanoparticles
Molecular formula	Fe <sub>3</sub> O <sub>4</sub>
Colour	Jet black
Density (g/cm <sup>3</sup> )	5.18
Melting point (°C)	1583–1597
Type of magnetism	Ferrimagnetic
Curie temperature (K)	858
Saturation magnetisation (M <sub>s</sub> ) at 300K [emu g <sup>-1</sup> ]	92–100
Standard Gibbs free energy of formation (ΔG <sub>f</sub> <sup>0</sup> ) [kJ/mol]	–1012.6
Crystallographic system	Cubic
Structure type	Inverse spinel
Lattice parameter (nm)	α = b = c = 0.8396
Lattice angles	α = β = γ = 90°
Band gap energy (E <sub>g</sub> ) [eV]	2.6

### 3. Synthesis of Magnetite (Fe<sub>3</sub>O<sub>4</sub>) Nanoparticles

Several approaches have been developed to synthesise MNPs. Synthesis methods are vital in acquiring nanoparticles with tailored properties; highly crystalline structure; dispersity type; magnetic properties and controlled morphology, shape, and size. Furthermore, the synthesis approach must be cost-efficient, a relatively simple process, environmentally friendly, and possess a high reproducibility rate [25].

The basic techniques involved in the synthesis of MNPs are microbial, physical, and wet chemical methods. Each route possesses its own advantages, disadvantages, and effects over different properties of MNPs [45]. The methods described in this section explained the predominant synthesis of MNPs and how to obtain MNPs with narrow-sized distribution and desired morphology and shape by varying the synthesis parameters.

#### 3.1. Co-precipitation Method

Co-precipitation method is one of the most widely utilised methods in the synthesis of aqueous phase because of its simplicity and efficiency [10]. This method was first pioneered by Massart et al. in 1981 [46]. It is generally conducted through alkalisation of metal precursors. The most famous one is the ageing of ferrous and ferric salts at a 1:2 stoichiometric ratio in NaOH base at ambient temperature and with the presence of a continuous inert gas flow. A typical example of magnetite formation (Fe<sub>3</sub>O<sub>4</sub>) is described in Equation (1) [25]:



The production of homogeneous nanoparticles via co-precipitation method is based on two distinct phases: (i) nucleation and (ii) growth [47,48]. The nucleation phase normally starts with crystalline particles precipitating from a supersaturated solution until the constituent species decreases, thus forming nanoparticle crystals. The nucleation process occurs for a very short period of time, whereas the slow-controlled growth phase takes place due to the diffusion of solute from the solution to the surface of the crystals. If the two phases are controlled and separated, i.e., nucleation and

crystal growth do not occur simultaneously, polydispersed nanoparticles formation could be highly avoided, resulting in the synthesis of highly monodispersed MNPs. The growth of the nuclei of the particles could be in highly narrow-sized distribution if the nuclei begin to form at the same time. Thus, the obtained particle size could be tuned only in the nucleation phase because it does not vary during the growth phase [25,49].

The co-precipitation method takes place mainly through a topotactic stage conversion root (Figure 6): akaganeite stage (crystal nucleus formation) to goethite stage (narrow-shaped nanoparticle formation).

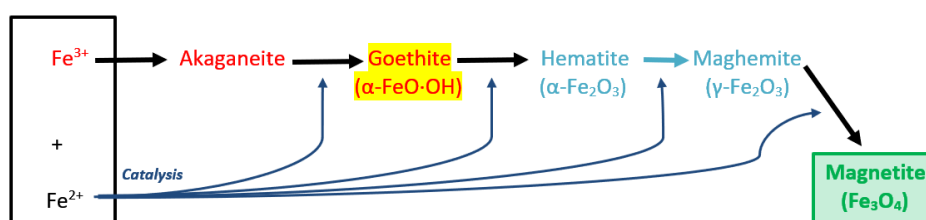


Figure 6. Formation root of MNPs via co-precipitation approach.

Goethite ( $\alpha$ -FeO·OH) is a mineral that is naturally found in soils. The focal intermediate stage is the goethite stage [2]. The stage from which magnetite converts into maghemite undergoes an oxidation process and the annealing of maghemite converts it into hematite.

Iida et al. synthesised MNPs via hydrolysis in an aqueous solution consisting of  $\text{Fe}^{2+}$  and  $\text{Fe}^{3+}$  salts at varying ratios and 1,6-hexanediamine was utilised as the base [50]. When the ratios of  $\text{Fe}^{2+}:\text{Fe}^{3+}$  were increased, huge OH (hydroxide) particles were formed as the precursor of magnetite was promoted. The size of the MNPs increased, with a mean diameter ranging from ~9 nm to ~37 nm. Furthermore, the magnetisation saturation value of the magnetite could be controlled by altering the ratio of  $\text{Fe}^{2+}$  and  $\text{Fe}^{3+}$  salts.

The concentration of Fe is an important contributor during the synthesis of MNPs, where the molarity values range between 39 and 78 mM [51]. During this synthesis, the precipitation below 60 °C leads to the production of amorphous hydrated oxyhydroxide, which easily oxidises into maghemite. The temperature should be kept to above 80 °C to stimulate the formation of MNPs [52].

A suitable pH for fast magnetite formation was achieved through excess amounts of base addition [1]. However, in this scenario, rapid formation of magnetite could also be attained with the usage of a strong base, such as sodium hydroxide, which has a much higher pH even at a much lower amount than a weak base, such as sodium carbonate [13]. The diameter of the synthesised MNPs could be controlled by alternating the concentration of the base (e.g., NaOH) and the pH values. At fixed pH, the size of the MNPs was directly proportional to the concentration of NaOH. When the concentration of NaOH was kept constant, the size of the MNPs was inversely proportional to the pH values. Thus, MNPs below the size of 3 nm were achieved at high pH and low NaOH concentration [12]. Blanco-Andujar et al. synthesised uncoated MNPs by using sodium carbonate as the base but their experiment resulted in a relatively slow reaction with less yield productions [53].

Few modified co-precipitation approaches have also been performed. For example, Wu et al. synthesised magnetite nanopowders with an average diameter size of 15 nm via ultrasonic-assisted chemical co-precipitation without the need for an inert atmosphere [54]. Pereira et al. developed a one-step aqueous co-precipitation route to synthesise superparamagnetic MNPs, with size ranging between 4.9 and 6.3 nm, by utilising alkanolamines, diisopropanolamine and isopropanol amine as the bases. This methodology is versatile, simple, and cost-effective for the synthesis of high-yield MNPs, with up to a six-fold reduction in particle and improvised saturation magnetisation of up to 1.3 times [55].

The bubbling of nitrogen gas into the sample prevents critical oxidation from occurring on MNPs. Nitrogen gas plays a vital role in particle size reduction compared with non-inert atmosphere [51].

However, saturation magnetisation of MNPs is crucially affected by synthesis parameters, such as reaction rate, stirring rate, base type, and base molarity [2]. Vikram et al. reported that the stoichiometric ratio of ferrous and ferric salts and base addition rate have influence in regulating the saturation magnetisation values of MNPs [56]. The variation in base concentration may yield nanoparticles with ferromagnetic addition rather than superparamagnetic. High yield synthesis of MNPs of up to 99% are possible as recently displayed by Wroblewski et al. [57]. The team managed to successfully show how to synthesize MNPs with 12.9 nm in average particle size that emits a saturation magnetization value of  $74 \text{ emug}^{-1}$ .

On the one hand, the main drawbacks of the co-precipitation approach are low crystallinity, polydispersion and size-broadened particle distribution. These drawbacks induce low-saturation magnetisation values ranging from  $\sim 30 \text{ emug}^{-1}$  to  $\sim 50 \text{ emug}^{-1}$  compared with  $92 \text{ emug}^{-1}$  of bulk magnetite [2,25]. Thus, the co-precipitation method is not a suitable route to attain highly monodisperses MNPs [49]. Another major drawback is agglomeration due to particle size at the micro/nanoscale. This phenomenon triggers high surface energy and enlarged specific surface area [51]. The control over composition, morphology, and the oxidation of MNPs are other drawbacks faced by this approach [13,25]. Moreover, the high pH of the reaction solution needs to be altered during and after synthesis (purification), thus producing very limited uniform and monodispersed MNPs [51].

On the other hand, the main advantage of co-precipitation synthesis is simplicity. It possesses much lower reaction rate and temperature than hydrothermal and thermal decompositions. In addition, using water as a solvent is eco-friendly, which also provides scalable and high-yield productions [1,49]. The co-precipitation method is one of the most successful and versatile routes for synthesising MNPs with high-saturation magnetisation value [13,25,49].

### 3.2. Solvothermal Method

Hydrothermal is also called solvothermal [1]. The difference is that the hydrothermal method utilises aqueous medium as the precursor, whereas the solvothermal method utilises organometallic compounds as the precursors [13,25]. Solvothermal synthesis includes different types of wet-chemical approaches of crystallising the substance in a sealed Teflon-lined stainless-steel autoclave at a temperature ranging from  $130 \text{ }^{\circ}\text{C}$  to  $250 \text{ }^{\circ}\text{C}$  under high vapor pressure ( $0.3\text{--}4 \text{ MPa}$ ) [13,25]. The solvothermal method is used to prepare ultrafine magnetite nanopowders, that is, shape-controlled, monodispersed, and high-crystalline MNPs [58]. This route is conducted to grow dislocation-free single crystal particles. The grains synthesised under this approach possess better crystallinity than those from other approaches [1,13].

Wang et al. used the solvothermal method to synthesise magnetite nanopowders [59]. They reported that magnetite nanopowders around the size of 40 nm could be synthesised at  $140 \text{ }^{\circ}\text{C}$  for 6 h. The synthesised nanopowders had a saturation magnetisation of  $85.8 \text{ emug}^{-1}$ , which was slightly lower than that of bulk magnetite.

Lin et al. used the solvothermal and hydrothermal methods to obtain hollow MNPs [60]. Ferric chloride (as iron source), urea, ethylene glycol (as reducing agent) and ammonium acetate were used to synthesise hollow magnetite spheres. Once the homogeneous solution was dispersed, the mixture was poured and sealed into a Teflon-lined stainless-steel autoclave and heated up to  $200 \text{ }^{\circ}\text{C}$  for 8–24 h. They obtained magnetite in the form of ferric ions on the surface of the hollow spheres.

Tian et al. carried out a facile synthesis on ultrafine monodispersed MNPs, with precision up to 1 nm (average diameter), via the solvothermal method [61]. They used  $\text{Fe}(\text{acac})_3$ , n-octylamine, and n-octanol as the iron source, reducing agent, and solvent, respectively. They obtained MNPs ranging from 4 nm to 6 nm by altering the volume ratios of n-octanol and n-octylamine, with the absence of  $\text{N}_2$  gas bubbling or reflux conditions. In synthesising MNPs, the solvothermal method is more convenient in terms of heat consumption than the thermal decomposition method as extremely high temperature is required.

Stoia et al. synthesised Fe<sub>x</sub>O<sub>y</sub> nanocomposites via the solvothermal approach to utilise the nanocomposites as adsorbents for the removal of methylene blue from an aqueous medium [62]. They used ferric chloride as the iron source, diethylamine as the precipitating agent and 1,2-propanediol as the solvent.

Some researchers have attempted to modify the hydrothermal method. For instance, Ahmadi et al. synthesised MNPs at low temperature of below 140 °C without the use of autoclave. However, the saturation magnetisation value of the resulted MNPs was inadequate at short reaction rate (less than 2 h) [63]. Whilst well-crystallised magnetite grains synthesised via the solvothermal method may induce high magnetic properties in MNPs, they also have narrowed cationic distribution, lessened superparamagnetic relaxation, and thinned surface layer. In addition, the saturation magnetisation of MNPs varies with different solvothermal method conditions, as mentioned earlier in the report of Ahmadi et al. [63]. This phenomenon is evidently due to the different crystallinity structures of MNPs [1].

Even though the solvothermal method is very versatile, one of its main drawbacks is the stagnant reaction kinetics at any given temperature. However, this drawback could be overcome by microwave heating, which escalates the kinetics of crystallisation [64]. This method is known as the microwave-solvothermal method. The appealing characteristics of this modified method is the intensively fast kinetic reaction for synthesis (up to two orders of magnitude) due to the localised superheating of the solution. This integration helps overcome the main disadvantage of the solvothermal process, that is, slow reaction rate and low-yield productions [63].

Iacovita et al. successfully synthesised highly crystalline magnetite nanocubes (MNCs) via solvothermal reduction by using polyethylene glycol (PEG) 200 as the solvent. The relationship between the concentration of MNCs dispersed in water and the specific absorption rate (SAR) values are inversely proportional. Applying a magnetic field amplitude of 60 kAm<sup>-1</sup> resulted in a SAR value of up to 1700 Wg<sup>-1</sup>. When the MNCs were immersed into PEG-600 (liquid) and PEG-1000 (solid), the SAR values were heavily decreased by 50% or 75%, indicating that the Brownian friction that occurred within the solvent was the main driver to the heating power of MNCs [65].

This report clearly showed that the heat dissipation capacity of MNPs heavily depends on the type of base used, which is the most important criterion for their usage in MHT because high thermal dissipation is needed in killing cancer cells. The other main advantage of the solvothermal method over other types of crystal formation route includes its ability to synthesise crystalline phases that are unstable at the melting point and materials with high vapor pressure near the melting point. In addition, this method produces good shape-controlled MNPs [63].

### 3.3. Wet-chemical Reduction Method

Amongst the different types of solution-phase chemistry approaches developed for the synthesis of MNPs, the reduction in metal salts, such as sodium borohydride, is the most widely used [1]. In the environmental indemnification field, nanosized zero-valent irons have been extensively prepared by mixing sodium borohydride and ferric chloride at an equal ratio. The main advantage of this route in synthesising MNPs is simplicity, similar to the co-precipitation method. It could be conducted safely in all chemical labs with easily obtainable chemical reagents under ambient conditions. The concentration of the reducing agent plays an utmost important role in this synthesis method. If the concentration of the reducing agent is too high, the iron oxide is directly reduced to maghemite (γ-Fe<sub>2</sub>O<sub>3</sub>) rather than magnetite (Fe<sub>3</sub>O<sub>4</sub>). Thus, the reducing agent's molarity is a highly important factor in this synthesis approach.

### 3.4. Micro-/nano-emulsion Method

Emulsion is a thermodynamically stable anisotropic liquid mixture dispersal in two immiscible oil-in-water (O/W) and water-in-oil (W/O) single-phase systems with the presence of an amphiphilic molecule (surfactant). MNPs prepared via the micro-/nano-emulsion method depend on the structure

and type of surfactant [66]. The most common type of surfactants used include sodium dodecyl sulphate (SDS), bis(2-ethylhexyl) sulfosuccinate (AOT), poly-vinylpyrrolidone, and cetyltrimethylammonium bromide (CTAB) [13,25]. Identifying which surfactant must be used depends on the physicochemical characteristics of the system [52]. Surfactant molecules create a monolayer film at the water/oil interface, where hydrophobic tails (surfactant molecules) dissolve in the oil phase and hydrophilic head groups (aqueous phase) and vice versa on the basis of the type of surfactant used. The product of this method is a transparent and stable solution [1,13,25,52]. The hydrophobic and hydrophilic section of surface coatings play a vital role in (i) stimulating chemical reactions to occur, (ii) controlling physicochemical parameters, and (iii) stabilising the nanoparticles [2]. In this method, the aqueous phase may consist of metal salt precursors and the 'oil' phase may consist of complex mixtures [13].

The two types of micro-/nano-emulsion techniques are direct micro-/nano-emulsion and reversed micro-/nano-emulsion. Direct micro-/nano-emulsion is where oil is dispersed into water (O/W), whereas reverse micro-/nano-emulsion is where water is dispersed into oil (W/O). Both methods have been used in the synthesis of uniform-sized and tailored-shaped MNPs [13,25]. Between these two methods, the reverse method is more frequently utilised in the synthesis of MNPs [2]. Figure 7 illustrates a schematic of a W/O micro-/nano-emulsion droplet.

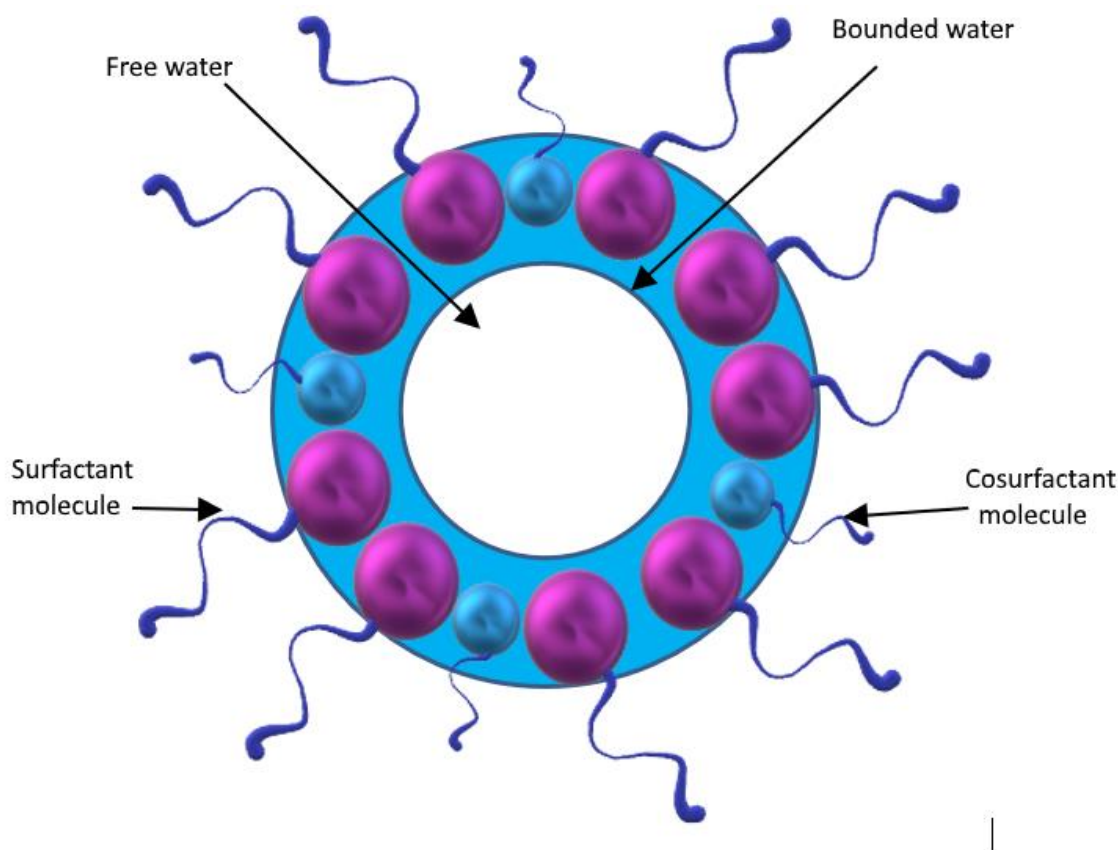


**Figure 7.** Schematic of W/O micro-/nano-emulsion droplet.

The size and dynamics of synthesised MNPs could be controlled by altering the following factors: concentrations of iron oxide precursor to base, solvents, and surfactants; droplet size; oil/surfactant/water; nature of surfactants; initial concentration of reactants; and reaction temperature and time [2,13,25].

Lu et al. revealed that surfactant plays a vital role on the final characteristics of MNPs [67]. They investigated the effect of dodecyltrimethylammonium bromide, CTAB (cationic surfactants), non-ionic surfactant and SDS (anionic surfactant) on the crystallinity, saturation magnetisation values

and stoichiometric situation of the resulted MNPs. They mostly obtained MNPs with sizes < 16 nm. However, with the use of cationic surfactants, they obtained MNPs with good magnetic properties, which are especially important in biomedical field application.

The main drawback of the micro-/nano-emulsion method is low-yield productions for such a large amount of solvent used [1,13,25]. Once the MNPs are formed, repeated purification processes are required due to aggregation and to remove excess amounts of surfactants with adverse effects [68]. Further stabilisation purifications are required for the MNPs to be utilised in the biological field [13]. These shortcomings make the micro-/nano-emulsion method quite a costly method to synthesise MNPs.

Overall, the micro-/nano-emulsion method could synthesise size-controlled monodispersed MNPs with uniform morphology at high saturation magnetisation values [1,25]. Compared with other methods, this method utilises simple equipment with ambient synthesis conditions. It also provides the high probability of synthesising a wide variety of MNPs with a high degree of control over composition and large specific surface area [53].

### 3.5. Sonochemical or Sonolysis Method

The sonochemical (sonolysis or ultrasound irradiation) approach utilises sound-to-chemical energy conversion to synthesise novel MNPs; acoustic cavitation produces bubbles via high-intensity ultrasound, which converts the reactants into desired MNPs at ambient conditions [69]. Acoustic irradiation operates with an ultrasound probe, such as a titanium horn functioning at 20 kHz [53]. In relation to ultrasound irradiation, the constantly varying compressive and expansive acoustic waves produce bubbles (i.e., cavities) and cause them to oscillate. The oscillating bubbles can effectively accumulate ultrasonic energy and the bubbles grow to a certain extent (~10 mm). At the right condition, a bubble can overgrow and subsequently collapse, releasing the stored kinetic energy within a very short period. This cavitation implosions with a pressure of ~1800 atm, a temperature of 5000 K and cooling rates in excess of  $10^{10}$  K/s are transient and well localised [13,53]. Volatile precursors in low vapor pressure solvents are normally utilise to improvise yield productions [53]. The shape and size of MNPs could be altered by controlling the irradiation time, power, and refluxing time [2].

Dolores et al. reported ferric ion productions utilising surfactant (ethylene glycol) to make IONPs. The relationship between the ferric ion production and the reaction time are directly proportional, particularly at ultrasonic frequency of 581 kHz rather than 861 and 1141 kHz [70]. The sonochemical approach could also be used to synthesise biocompatible MNPs. For example, Theerdhala et al. investigated semi-essential amino acid (L-arginine) binding with the surface of MNPs, creating a stable aqueous suspension. These coated MNPs may become a potential candidate for drug delivery application [71]. Zhu et al. synthesised uniformly dispersed MNPs, with sizes ranging from 30 nm to 40 nm, on a reduced graphene oxide sheet ( $\text{Fe}_3\text{O}_4/\text{RGO}$ ). The composite was immobilised with haemoglobin for the fabrication of a biosensor that detects hydrogen peroxide. The device displays an agile response towards hydrogen peroxide within few seconds [72].

In addition, the ultrasound-initiated method is an efficient approach to produce nanocomposites consisting of various polymers and encapsulated materials. Teo et al. came up with an effective and simple approach of preparing 100 nm-latex beads packed with highly loaded MNPs. The synthesised MNPs exhibited excellent superparamagnetic properties with a saturation magnetisation value of  $24 \text{ emug}^{-1}$  and high colloidal stability [73].

The sonolysis approach has some advantages, including fast chemical rates and dynamics of the reactions and uniformity mixture. The MNPs obtained using this approach are also homogeneous in size and shape particles [13].

### 3.6. Green Method (Biosynthesis)

In recent years, *green* nanotechnology has become the main attention of researchers due to the reduction in or elimination of toxic substances for environmental restoration and sustainability. The biosynthesis of MNPs is similar to a bottom-to-top method [74]. Researchers biosynthesised

metal nanoparticles by using exudates [75], plant extracts [76], inactivated plant tissue [77], and other parts of living plants [78]. In addition, microorganisms [79] have been included as a potential substance for the preparation of nanoparticles via the biological method. The microorganisms here refer to iron-reducing bacteria and magnetotactic bacteria, such as *Magnetospirillum gryphiswaldense* and *Geobacter metallireducens*. They have been used in traditional biosynthesis of MNPs [74]. Plant phytochemicals or microbial enzymes naturally contain antioxidants or also known in chemistry term as reducing agents, such as ascorbic acids, citric acids, dehydrogenases, extracellular electron shuttles, flavonoids, and reductases. Plants were selected for the biosynthesis of M-IONPs because plants may have a great potential to act as reducing agents during synthesis [80,81].

Awwad A. M. and Salem N. M. reported a facile, non-toxic, rapid, and green synthesis approach to synthesise MNPs via a one-step single-vessel reaction. The used  $\text{FeCl}_3 \cdot 6\text{H}_2\text{O}$ ,  $\text{FeCl}_2 \cdot 4\text{H}_2\text{O}$ , NaOH, and carob leaf extract [82] and obtained monodispersed MNPs with an average diameter of 4–8 nm at a relatively low temperature (80–85 °C). The synthesised MNPs were surface-functionalised with carboxylic groups of amide I and amide II chains sourced from the protein in carob leaf extract.

Sundaram et al. investigated the capability of *Bacillus subtilis* strains segregated from rhizosphere soil to synthesise stabilised MNPs, which were coated with organic molecules. This approach was successful, indicating its applicability to synthesise in bulk amounts [83].

Chin et al. synthesised narrow-sized distributed and size-controlled MNPs via thermal decomposition approach by using poly(ethylene glycol) (PEG) as the surfactant and solvent simultaneously [84]. PEO is also known as a green solvent due to its non-toxic property. It has been used in several biosynthesis as a substitute for organic solvents [85]. It has also been used to reduce the agglomeration of MNPs [84].

Aside from chemical compounds, plant extracts could be used as stabiliser. M. Nurbas and co-workers successfully biosynthesise MNPs by using *Platanus Orientalis Linnaeus* plant leaves as water extracts, which serve as an excellent capping agent and stabiliser. Zetasizer (also known as particle size analyser) results showed that the biosynthesised MNPs have a hydrodynamic radius of around  $35 \pm 7$  nm [86]. Omidvari et al. similarly biosynthesised superparamagnetic MNPs with an average diameter ranging between 30 to 40 nm by employing the extract of *Acanthophyllum Bracteatum* as the surfactant in Soxhlet extraction [87].

Plant extracts are not only used as functionalising agents and stabilisers but also as reducing agents in the synthesis of MNPs. Yen Pin Yew et al. successfully synthesised mostly spherically shaped MNPs of 14.7 nm in average size by employing seaweed (*Kappaphycus alvarezii*) as a green stabilising and reducing agent [88].

Elisa Rasouli et al. recently used natural honey at varying percentages (*w/v*) as capping and reducing agent to synthesise spherical MNPs. After they reduced the percentage of natural honey, the saturation magnetisation values increased, as shown by the VSM results. They conducted in vitro feasibility appraisal on WEHI164 cells through MTT and showed significantly non-toxic properties at high concentration reaching 140 ppm. Their findings suggested that these green-synthesised MNPs are important in biological applications, such as TDD, MRI, and biosensors [89].

In another recent report, M. Temelie et al. studied the biocompatibility of MNPs obtained via an eco-friendly, facile, and novel way by using a turmeric-aided technique. They used normal fibroblasts (L929 cell line) for the in vitro biocompatibility assay and revealed a negative genotoxic effect and no induced cellular death. The obtained results were further concretised through haemolysis analysis that showed negative erythrocyte lysis. Their results proved that the obtained MNPs are non-toxic and could be applied in several biological fields [90].

Given their biocompatible properties, these end-product MNPs has a great potential in biomedical applications. The reported drawback of the green approach is that the MNPs produced have poor shape and the ability to control their size during biosynthesis is limited. Overall, this method requires further substantial experiments and investigations. In conclusion, the green synthesis of MNPs is biocompatible, environmentally friendly, non-toxic, reliable, and safe for biomedical applications [81].

### 3.7. Summary

Table 3 summarises and compares all of the synthesis methods of MNPs discussed. It would be quite impossible to choose just one as the optimum synthesis method for biomedical applications. However, each synthesis method has a different but significant impact on specific biomedical application. For example, high porosity is an important factor in drug-loading for TDD application. In this case, the best method is the solvothermal technique, where high temperature and pressure are required to synthesize porous MNPs. As for MHT, the shape of MNP is important in order to generate high SAR values upon the application of an AMF. Therefore, solvothermal or micro-/nano-emulsion methods are more favourable due to their ability to control the MNP's shape. Eventhough solvothermal methods are suggested in both aforementioned applications, it is one of the most expensive method as compared to the others at an industrial scale. Due to this, most researchers would prefer methods such as co-precipitation and green (biosynthesis) for their cost-efficiency.

**Table 3.** Comparison summary of MNP synthesis methods.

Methods	Reaction	Condition	Reaction Temp. (°C)	Reaction Period	Size Distribution	Shape Control	Yield
Co-precipitation	Very simple	Ambient	20–150	Minutes	Relatively narrow	Not good	High/scalable
Solvothermal	Simple	High pressure	150–220	Hours–days	Very narrow	Very good	High/scalable
Wet-chemical Reduction	Very simple	Ambient	20–150	Minutes	Relatively narrow	Not good	High/scalable
Micro-/nano-emulsion	Complicated	Ambient	20–80	Hours	Narrow	Good	Low
Sonochemical/Sonolysis	Very simple	Ambient	20–50	Minutes	Narrow	Bad	Medium
Green (Biosynthesis)	Complicated	Ambient	Room temp.	Hours–days	Broad	Bad	Low

## 4. Surface Functionalisation of Magnetite (Fe<sub>3</sub>O<sub>4</sub>) Nanoparticles

The main issue of MNPs concerning their size scales is long-term inherent instability, which occurs in two main routes: (1) dispersibility loss, where bare MNPs tend to agglomerate due to Van der Waals forces, overcoming the high surface energy and the strong magnetic attraction between particles [91]; and (2) magnetism loss, where oxidation of MNPs occurs. These issues can be handled by developing a functionalised surface around the surface of MNPs to enhance biocompatibility and hydrophilicity. Encapsulation of MNPs prevails agglomeration by reducing the surface area formed, thus indirectly reducing the surface energy for agglomeration to occur. It also creates a protective layer around bare MNPs, preventing MNPs from going through oxidation as they oxidise to maghemite ( $\gamma$ -Fe<sub>2</sub>O<sub>3</sub>) upon long period of exposure to air. This step retains the magnetic characteristics of MNPs. Introducing a coated shell on the surface of MNPs ensures the chemical stability of bare MNPs.

Coated MNPs have various advantages over bare MNPs in biomedical applications, including reduced cytotoxicity, increased cyto-compatibility and increased bio-conjugation. In terms of the core of MNPs, the composition of the shell provides biocompatibility and bio-conjugation properties due to the presence of reactive materials on its surface [91,92]. The thickness of the shell could be tailored to provide sufficient contrasting properties (contrasting agents) and biomolecule binding for TDD and biosensing purposes [92]. Figure 8 illustrates a schematic of various biomedical applications of core/shell MNPs.

Organic polymers and inorganic materials are most commonly utilised for the encapsulation of bare MNPs. An example of organic functionalisation is the usage of natural polymers (polysaccharides and proteins/polypeptides) and synthetic polymers are extensively used for imaging and cancer therapy. The main reason polymeric systems are popular capping agent is due to their sensitivity towards temperature and pH, which favours drug release at the cancer site [93,94]. For inorganic materials, silica is the most commonly used capping agent by researchers. This capping process could be prepared through various synthesis approaches, but the surface-functionalised MNPs must be in

definite sizes to avoid them from passing through the kidneys and being accumulated at the liver and spleen [2,38,95,96].



**Figure 8.** Various biomedical applications of core/shell MNPs.

#### 4.1. Organic Functionalisation

Several techniques have been developed to encapsulate MNPs, including post-synthesis and in situ encapsulation, which are amongst the commonly utilised approaches for organic material encapsulation on the surface of MNPs [97,98]. Some of the most commonly used organic materials in the surface functionalisation of MNPs include dextran, poly(D,L-lactide) (PLA), PEG, polyethylenimine, and starch. These examples are mostly hydrophilic.

##### 4.1.1. Surfactants and Small Molecule

The major advantage of small molecular coatings of MNPs is that huge (>50 nm) hydrodynamic size could be overcome. MNPs could be functionalised with special groups, such as  $-\text{COOH}$ ,  $-\text{NH}_2$ ,  $-\text{OH}$  and  $-\text{SH}$ , which have a potential for further modifications with various bioactive molecule attachments. Shen et al. reported a facile technique to synthesise 3-aminopropyltriethoxysilane (APTES)-coated magnetite with tailored surface functional groups to be applied in the biological field. Haemolytic assay and cytotoxicity results showed that the acetylation of amine groups on the surface of MNPs notably ameliorates the hemocompatibility and cytocompatibility [99]. In addition, as observed in past research, mercaptopropyltriethoxysilane (MPTES)-modified MNPs trigger a minute decline in magnetic properties, whilst APTES helps maintain the morphology of MNPs. Recently, Dheyab et al. managed to successfully synthesise highly magnetized and 19 nm-sized citric acid-functionalised MNPs by employing a rapid and simple one-step co-participation method. The results portrayed a  $54.8 \text{ emug}^{-1}$  magnetic saturation [100].

The functionalisation of oil-soluble type MNPs are also essential in yielding monodispersed MNPs. Oleyamine and oleic acid are the most widely used organic compounds in the synthesis of this type of MNPs. They possess a C18 tail with a *cis*-double bond in between that forms a kink. These kinks

are substantial for efficient stabilisation, which explains why stearic acid is incapable of stabilising M-IONPs (absence of double bond in its C18 tail) [13]. Furthermore, oleic acid is commonly used in the synthesis of IONPs due to its ability to form a dense protective monolayer that stimulates highly uniform IONPs.

Oleyamine and oleic acid are frequently utilised in high-temperature thermal decomposition synthesis. For example, magnetite was synthesised via facile thermal decomposition of  $\text{Fe}(\text{acac})_3$  with oleic acid [101,102]. Oleic acid-coated MNPs showed no significant variation in the overall magnetic behaviour of samples. These MNP systems with high saturation magnetisation values correlate up to 80% of the bulk value and could be applied in the biomedical field [13]. Using small molecules, such as citric acid, amino acid, cyclodextrin, vitamin and many others, is necessary to synthesise water-soluble MNPs. Gao et al. synthesised eminently charged hydrophilic superparamagnetic magnetite colloidal nanocrystal clusters via a modified one-step solvothermal method, which resulted in an average diameter of ~195 nm. They used anionic polyelectrolyte poly(4-styrenesulfonic acid-co-maleic acid) sodium salt as the stabiliser [103].

#### 4.1.2. Polymers

Polymer encapsulation is highly favourable in synthesising biocompatible and colloidal water-soluble MNPs [10]. The two main types of polymers heavily used in the coating of M-IONPs include synthetic polymers and natural polymers. Between these two, synthetic polymers are excessively used in encapsulating MNPs. Their functionalisation are sophisticated in synthesising a new type of di-block copolymers or tri-block copolymers through various polymerisation techniques for MNP functionalisation. Ali et al. synthesised janus-like MNPs by manipulating poly(methylmethacrylate-acrylic acid-divinylbenzene), which was assembled using emulsion polymerisation technique. The janus-like synthesised MNPs had sizes ranging between 200 and 250 nm [104]. This range could be attributed to the reduction of interfacial energy between the magnetic domain of the nanoparticle and polymer, resulting in a single-dimension MNP growth.

#### 4.1.3. Biomolecules

Biomolecule encapsulation has been used in sensing, biological separation, and other biomedical applications due to its superior biocompatibility properties. The different types of biomolecules include antibodies, avidin, biotin, enzymes, human serum albumin, polypeptides, and proteins [105–109]. Bhattacharya et al. used antibody-labelled multifunctional gold-magnetite nanocomposites to detect *Staphylococcus aureus* at ultra-low concentration [110]. Fluorescence and optical microscopy detected  $10^2$ – $10^7$  CFU  $\text{mL}^{-1}$  concentrations of *S. aureus* in 30 min within a detection limit of  $10^2$  CFU  $\text{mL}^{-1}$ . These antibody-loaded nanoparticles are important sensing agents for wide application in probing a certain type of bacteria (*S. aureus*) in diverse biosensing systems. In conclusion, highly biocompatible, biomolecule-modified M-IONPs could be the best candidate in bioseparation applications for cells, DNA, and proteins.

### 4.2. Inorganic Functionalisation

Inorganic materials for functionalisation have several advantages, such as great magnetic moment (e.g., Mn and Co), powerful optical absorption and high electron density (e.g., gold and silver) [13,111]. Similar to organic encapsulation, inorganic encapsulation provides colloidal stability in aqueous medium and biological labelling capability, where gold and silica help in binding different types of biological ligands on the surface of MNPs [112–114].

#### 4.2.1. Silica ( $\text{SiO}_2$ )

Silica-functionalised MNPs ( $\text{MNP@SiO}_2$ ) is a nanocomposite often used in colloid surface encapsulation. The silica shell surface is compatible with various molecules and chemicals for further bioconjugations [115].  $\text{SiO}_2$  functionalisation accumulates in an aqueous medium due to the ability

of the SiO<sub>2</sub> layer to screen the magnetic dipolar attraction between magnetic MNPs. Moreover, SiO<sub>2</sub> functionalisation shields the MNPs in an acidic environment and enhances their stability at the same time. In addition, the attachment of various functional groups and ligands covalently on the surface of silica is less complex due to the presence of abundant silanol groups on the SiO<sub>2</sub> layer [10,13].

In terms of practicality, MNPs should be encapsulated with a homogeneous SiO<sub>2</sub> layer without core-free silica particles. These silica-coated MNPs function as a magnetic guidance and a drug-loader simultaneously and as biomarkers; they are also used for dye labelling for TDD and hyperthermia therapy [10,13]. The density of SiO<sub>2</sub> shell could be tailored by altering the reaction conditions to either dense or porous. During the synthesis of SiO<sub>2</sub> functionalisation, octadecyltrimethoxy silane, tetraethyl orthosilicate (TEOS) and vinyltriethoxysilane are amongst the frequently utilised silanes with the presence of MNPs. These silanes effortlessly bind on the surface of MNPs via the OH groups [10,116–118].

The most common approach used in the generation of MNP@SiO<sub>2</sub> nanomaterials is the well-known Stöber method [119]. SiO<sub>2</sub> is synthesised in situ via hydrolysis and condensation of a sol-gel precursor. The Stöber method is a multi-versatile approach used in aqueous and organic media. It is also one of the most prominent techniques for obtaining MNP@SiO<sub>2</sub>. Gao et al. prepared magnetite@silicon-dioxide nanoparticles by using 20-nm hydrophilic MNPs as seeds [115]. The experimental parameters, such as the concentration of magnetite seeds, ratio of TEOS/magnetite and reaction time, were tuned, which was found to be crucial in tailoring the thickness of the silica shell from 12.5 nm to 45 nm. In a previous study, ultrafine hollow magnetite/silica nanoparticles with a large surface area and a diameter of around 32 nm were prepared, with CTAB and AOT as co-templates, followed by subsequent annealing treatment [120]. These as-prepared magnetite@silica nanoparticles are commonly used in MRI. The thicker the SiO<sub>2</sub> shell, the lower the  $r_1$  and  $r_2$  relaxivities [121]. In the Stöber method, the amount of silane used is an important factor in altering the thickness of SiO<sub>2</sub> shell, which could be used as an enhanced contrasting agent for targeted biomolecules [92].

The other method in the preparation of MNP@SiO<sub>2</sub> is the microemulsion synthesis [122]. This approach is more complex in segregating the core@shell from a huge number of solvents. Ding et al. investigated the encapsulation regulations of MNPs through reverse microemulsion approach to synthesise magnetite@silica nanoparticles [123]. However, the microemulsion synthesis system offers a more controlled environment for obtaining uniform SiO<sub>2</sub> coatings with the ability to control the thickness of the coating.

#### 4.2.2. Carbon

The usage of carbon as a coating material on the surface of MNPs has been recently discovered and favoured in the research communities due to its superior properties, such as high intrinsic electrical conductivity, thermal and chemical stability, protection of the magnetic core from corrosion and ability to act as an oxidation repellent. In addition, MNP cores coated with hydrophilic carbon encapsulation have proficient stability and dispersibility compared with bare MNPs [124]. Several methods have been developed for the synthesis of MNP@C core nanostructures. The commonly used approach is a three-step approach, where the as-prepared MNP seeds through various techniques go through polymerisation. The surfaces of the MNPs are functionalised with polymer, which is then annealed to form MNP@C composite materials (Figure 9).

Li et al. demonstrated, for the first time, that the structural transformation of eccentric Fe<sub>2</sub>O<sub>3</sub>@poly(acrylic acid) core-shell nanoparticles could synthesise selection-controlled, monodispersed magnetite@carbon core-shell chains, rings and spheres with alterable magnetic properties and sheer scale [125].

Focus has been given to the synthesis of MNP/graphene as the latest type of hybrid material, contributing to its applications in the biomedical field, such as in MRI and TDD [126–128]. For instance, Chen et al. reported that functionalised composites of aminodextran-encapsulated MNPs and graphene oxide were effective for cellular MRI. In comparison to bare MNPs, MNPs@graphene oxide composites

have a notably  $T_2$ -weighted MRI contrast due to the aggregation of MNPs on the graphene oxide sheets, thus resulting in hiked-up  $T_2$  relaxivity [129].

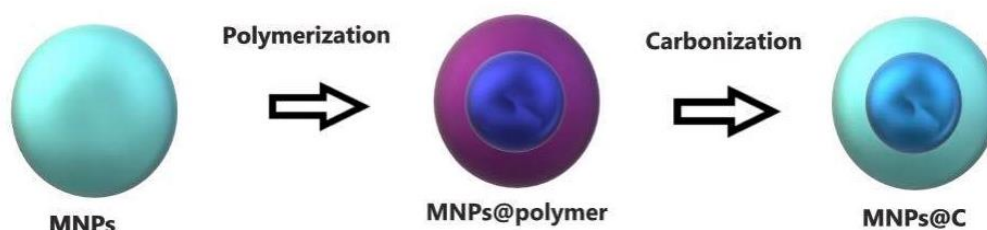


Figure 9. Fabrication process flow of MNP@C.

Zhu et al. embedded MNPs into a carbon substrate utilising ethylene glycol photoresist as the source of carbon [130]. They prepared MNPs through the thermal decomposition approach, followed by layer-by-layer assembly, to synthesise MNPs embedded with photoresist on a silicon substrate. The as-prepared substrates showed a low temperature annealing that resulted in a carbon-encapsulated silicon substrate. They could be used for the growth of nerve cell PC12, where the adhesion ability of the substrate towards the cells is in congruence with the concentration of MNPs.

In another study, MNPs with a thin carbon coating were successfully synthesised via thermal decomposition method, where iron oleate was utilised as the precursor [131]. Solvents, such as docosane, eicosane, octadecane, and octadecene, were used to vary the temperature of the thermal decomposition process and docosane achieved the highest temperature at 365 °C. The thin carbon shell was functionalised through oleate ligand carbonisation. These newly coated MNPs influence cytotoxicity [10,131].

However, carbon-coated MNPs possess certain disadvantages. Most of the carbon coating synthesis methods normally require a high-temperature annealing process, which carbonises hydrocarbon precursors whilst stimulating the reduction in IONPs. For example, annealing magnetite ( $\text{Fe}_3\text{O}_4$ ) nanoparticles at 700 °C reduced MNPs into hematite ( $\alpha\text{-Fe}_2\text{O}_3$ ) nanoparticles (HNPs) [132]. Even though HNPs are more stable than MNPs at room condition, the high temperature annealing process drastically reduce the magnetisation saturation values, which are undesirable to biological applications [10,132].

## 5. Biomedical Applications of Magnetite ( $\text{Fe}_3\text{O}_4$ ) Nanoparticles

MNPs have a great potential in the biomedical field (i.e., diagnosis). Given their nano-scaled size, they are very compatible with cells. The biomedical application of MNPs is enforced with strict parameter specifications, including chemical composition; flexibility and hardness; granulometry; homogeneous crystal structure; pore volume; adsorption, magnetic, pharmacological, and physical properties; size; solubility; structure and surface area; and uniformity [133–135]. The parameters determining biocompatibility are the characteristics of magnetically reactive MNPs. A high saturation magnetisation value enables MNPs to mobilise within the blood stream in the presence of an external magnetic field until they reach close enough to the targeted pathologic tissues [136].

The biomedical applications of MNPs can be divided on the basis of their applicability, whether they are inside the body (in vivo) or outside the body (in vitro). In vivo applications can be further classified into diagnostic (MRI) and therapeutic (hyperthermia and TDD) applications. In vitro applications mainly deal with diagnostic separation, magnetorelaxometry and selection [1,135].

### 5.1. In Vivo Applications

The two main factors that need to be considered in the usage of MNPs in vivo include size and surface modification. MNPs possess huge surface area that can be surface functionalised with a huge quantity of functional groups for crosslinking to tumour-targeting ligands, diagnostic imaging, or therapeutic agent delivery [137]. The diameters of MNPs primarily affect their performance in vivo,

even in the absence of tumour-targeting surface ligands. A diameter ranging around 10–40 nm is utilised in various applications, such as in cross capillary walls and prolonging blood circulation [1].

The usage of MNPs in *in vivo* can be classified into three categories; (i) magnetic vectors that could be driven towards tumour-targeted tissues through a gradient of magnetic field; (ii) magnetic CAs in MRI; and (iii) magnetic hyperthermia, where heat is generated by the application of high-frequency AC magnetic field that causes thermo-ablation of cancer cells [12]. In recent years, due to the advancement of technology in the biomedical field, there are also reports on the combination of *in vivo* applications simultaneously, like the usage of both TDD and MHT [138], and also MHT and MRI [139]. This section discussed recent studies on TDD, MRI, and magnetic hyperthermia, which are the three most common *in vivo* applications driven by MNPs.

### 5.1.1. TDD

Traditional TDD, such as intravascular injection and chemotherapy, depends on the systemic blood circulation to distribute anticancer drugs throughout the body, especially tumour tissues. However, only a minuscule amount of dosage reaches these tissues. Moreover, issues on the toxicity of drug attack in healthy tissues are present. Given these drawbacks faced by patients and doctors, TDD has been introduced as a replacement for the traditional chemotherapy treatment [5,140].

TDD has become one of the most sophisticated technologies in cancer therapy. It focuses the loaded drugs on the cancer site, controls the amount of drug flow towards the tissues of interest and reduces the side effects [5,134,140]. The application of MNPs in TDD has increased tremendously over the years [141]. MNPs are generally functionalised with biocompatible materials, such as polymers or gold. Functionalisation is carried out to ensure the anticancer drug could either be loaded within the MNPs or conjugated on the surface of MNPs, as shown in Figure 10 [142]. Once the drug is loaded (drug-loaded MNP), an external magnetic field is utilised to guide the drug-loaded MNP to the desired cancer site. The drug release is influenced by various factors, such as osmolality, enzymatic activity, changes in pH, temperature, electromagnetic trigger, and dual or poly-sensitivity [143–145].

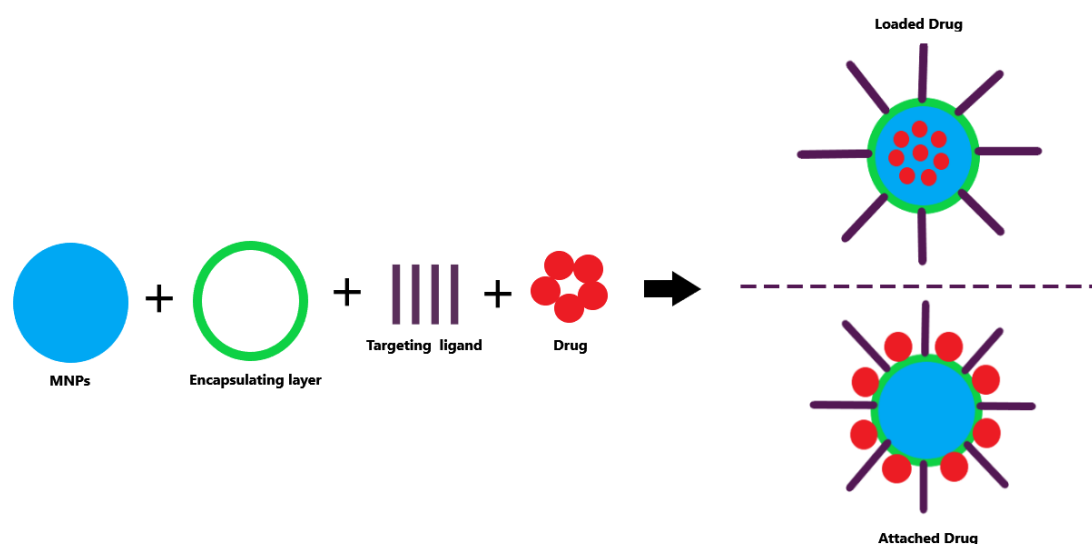


**Figure 10.** Illustration of drug loading roots in TDD.

High drug loading and fast drug-release efficiency are important parameters in the drug delivery system. Mesoporous surfaces, such as carbon and  $\text{SiO}_2$ , have a good ability to promote and increase drug-loading capability [140]. Zhang et al. investigated the advancement of a magnetic drug carrier made up of doxorubicin-conjugated MNP cores and a PEG-encapsulated porous silica layer ( $\text{Fe}_3\text{O}_4\text{-DOX@pSiO}_2\text{-PEG}$ ). This porous drug carrier system has a DOX-loading capacity of 16.3  $\mu\text{g}/\text{mg}$ . The magnetic drug carrier could be consumed by cells via endocytic process [146].

Haijuan et al. developed hollow microspheres of  $\text{Fe}_3\text{O}_4/\text{SiO}_2$  core/shell with the magnetic core as magnetite and PEG–PLA as the encapsulating layer ( $\text{Fe}_3\text{O}_4/\text{SiO}_2@\text{PEG-PLA}$ ) for TDD treatment. This synthesised ternary nanocomposite possessed various advantages in the TDD therapy. For instance, the hollow structure of the nanocomposite enables it to load drug at a great scale and its high saturation magnetisation value enables it to be directed with a magnetic field. The nanocomposite was biocompatible and biodegradable due to PEG–PLA [147].

Considering the strong magnetic strength of MNPs, they also possess excellent target specificity to the lesion tissue. Therefore, MNPs are more preferred by biomedical researchers in the field of TDD than other materials.

### 5.1.2. MRI

MRI is one of the most well-known biomedical imaging techniques in diagnostic medicine. It is applied primarily to generate high-resolution images of human tissues in 2D and 3D spaces. MRI functions on the principle of nuclear magnetic resonance. However, it requires a CA to increase its sensitivity sharpness for the detection of different kinds of pathological processes. MNPs in the superparamagnetic domain function as a good and reliable CA in in vivo applications due to  $T_1$  and  $T_2$  relaxation time and a high proton magnetic moment alignment time that results in a much-improved MRI image [27]. Upon exposure to an external magnetic field, MNPs produce gradients with large microscopic area. The microscopic field gradient reduces the relaxation time of nuclear spins ( $T_2^*$ ,  $T_1$  and  $T_2$ ), thereby resulting in a negative or dark contrast in  $T_2$ -weighted images. MNPs are less toxic and possesses high colloidal stability in a biological environment. Further enhancement of these properties in MRI application requires these MNPs to be functionalised into CAs.

Specific cell labelling or cell tracking is another niche possessed by MNPs in the field of MRI. In vivo labelling and cell tracking aim to study and observe cell therapeutics and biological processes, respectively. They monitor cell movement and provide molecular information about the viability and functionality of the cells. MRI provides resolution as minuscule as the size of the cell when the cells are loaded with highly sufficient amounts of MNPs.

In the study of MRI diagnosis, researchers have utilised several techniques that involved surface modification for MNPs [148–150]. Smolensky et al. showed that the integration of a thin organic shell consisting of IONPs and gold chelators significantly increased the magnetic property value of IONPs@gold core–shell. This phenomenon resulted in a plasmonic behaviour and MNPs@organic@gold nanocomposite with high relaxivity, which is a susceptible replacement for the current magnetoplasmonic agent used for multimodal cell imaging [151]. Zhou et al. also synthesised monodispersed Au@MNP@C core–shell nanospheres with hollow core diameters ranging around 50 nm. The nanocomposite was made up of Au@SiO<sub>2</sub> coated with a double layer of MNP@C and it finally dissolved into SiO<sub>2</sub>. The presence of gold and MNP enhanced the nanospheres, with dual probing ability for MRI diagnosis [152].

Gonzalez-Rodriguez et al. recently synthesised magnetite nanocrystals into hollow silicon nanotubes (SiNTs) as CA for MRI [153]. MNPs of 5- and 8-nm in average size were loaded into SiNTs of 40 and 70 nm-wall thicknesses (Figure 11). The nanocomposites were further functionalised through an aminopropyl linkage with PEG-diacid (600) to attain acceptable colloidal stability. The relationship between the relaxometry values of  $R_2$  and the nanocomposite shell thickness were inversely proportional. This study showed how the relaxometry properties could vary on the basis of the role of SiNTs.

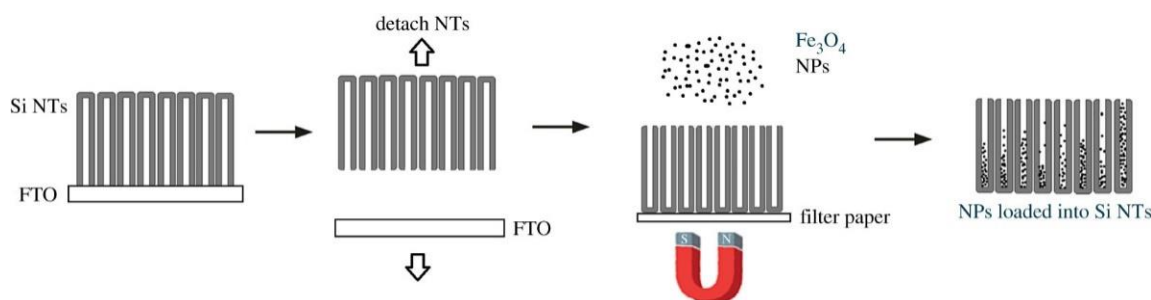


**Figure 11.** Schematic of MNPs being loaded into SiNTs [153].

Ardelean et al. demonstrated a facile co-precipitation approach to prepare mesoporous MNPs through various stabilising agents, such as glutamic acid, salicylic acid and trichloroacetic acid [154]. Stabilising agents are utilised to prevent aggregation of MNPs. These resulting MNPs are potential candidates for CAs, indicating the high candidacy potential of MNPs as primary MRI agents in theranostic and imaging procedures for the detection of tumour tissues. MNPs do not need to function as the primary delivery carrier for therapeutics due to their low  $R_2:R_1$  ratio and high  $R_2$  relaxivity.

The superparamagnetic behaviour of MNPs makes them a promising CA for MRI application compared with their counterparts. In addition, MNPs easily bond to natural biomolecules, further increasing their potential to be used as CAs in MRI.

### 5.1.3. MHT

Hyperthermia is one of the most promising biological applications of MNPs in cancer therapy. It is a therapeutic approach whereby heat is induced to kill tumours [155,156]. MNPs act as thermal seeds. Once MNPs are localised using an external magnetic field, MNPs were heated up under a high frequency alternating magnetic field (AMF) at  $\sim 1$  MHz [2] due to hysteresis loss. The temperature of the tumour cells is increased to 42–45 °C to annihilate tumour tissues without affecting the healthy ones due to the higher sensitivity to heat of cancer cells than normal cells. When the heating of the cancerous cells and tissues reaches around 42–45 °C, the cancerous cells undergo cell apoptosis (i.e., hyperthermic effect). If the heating of the cancerous tissues reaches  $>48$  °C, the tissues undergoes necrosis (i.e., thermo-ablation) [5,155,156].

The degree of heat dissipation given out by MNPs for magnetically mediated hyperthermia heavily depends on the anisotropy (magnetocrystalline or shape), magnetic field parameters, saturation magnetisation values and size [1,2,13,134,157]. The three types of hyperthermia therapy include local, regional, and whole-body hyperthermia. Local hyperthermia therapy focuses on a specific targeted site of the body part, regional hyperthermia therapy is usually targeted on large tissue areas (e.g., limbs and organs), whilst whole-body hyperthermia therapy is generally applied to treat metastatic cancer that has spread throughout the body. Amongst them, local hyperthermia therapy is the most prominently utilised method in modern MHT [5,13,158]. Figure 12 shows an illustration of the process of MHT.

Specific loss power and specific absorption rate (SAR) are the two primary parameters that quantitatively and qualitatively determine the efficiency of MNPs in heat dissipation resulting from the strength of the applied magnetic field [157,159]. SAR could be calculated analytically from the integration of the hysteresis loop (area of the hysteresis loop), but the process is quite tedious. The Brownian and Néel relaxation of the magnetic domains are massive contributors towards local heating of MNPs and a significant solution for localised hyperthermia therapy [157,160].

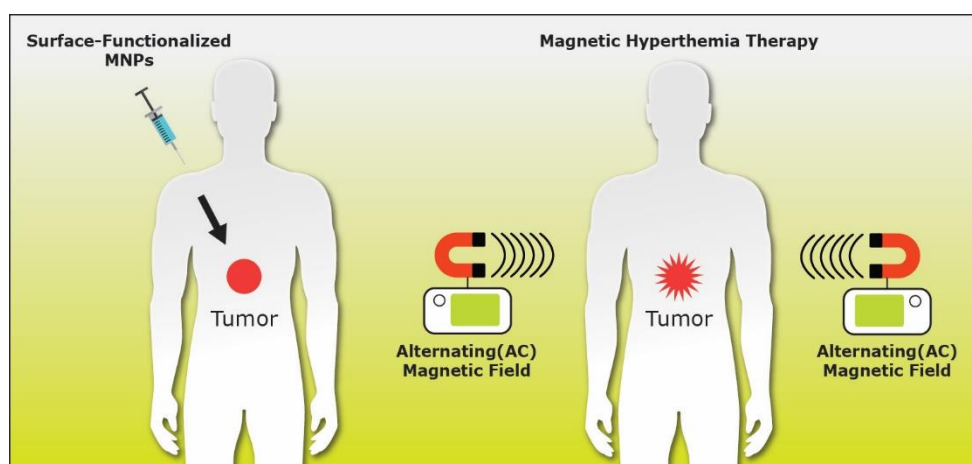


**Figure 12.** Illustration of a typical magnetic hyperthermia therapy process.

Hysteresis loss and Néel relaxation of the magnetic moment are the two highly dependent factors for localised hyperthermia therapy, with utilisation of AMF [161]. SAR is defined as the absorption rate of electromagnetic energy ( $E_{em}$ ) by a unit mass of MNP ( $m$ ) under the influence of an AMF. The expression of SAR is as follows:

$$SAR = \frac{d(E_{em})}{dt(dm)} \quad (2)$$

Superparamagnetic MNPs are amongst the best materials used in MHT. They are able to give a preliminary rise in temperature of 5 °C in just around 10 min [162]. Macías-Martínez et al. have synthesised superparamagnetic MNPs ranging from size 8 nm to 12 nm by using a simple co-precipitation approach. Under low magnetic field, the temperature increased to up to 43.1 °C in 5 min [163]. This finding made MNPs a very good candidate for MHT.

Localised hyperthermia therapy using surface-modified MNPs has been previously reported. Hayashi et al. demonstrated polypyrrole functionalised MNPs with a SAR value of 487 Wg<sup>-1</sup> [164]. The nanocomposite hindered the myeloma tumour injected into female mice to grow further. The tumour cells were completely destroyed when the nanocomposite was incorporated with 5 mg/kg of the chemotherapeutic drug. In a similar fashion, a 63 kHz AMF with 7 kA/m as amplitude value was induced on 0.1 mL of magnetic fluid consisting of 50 mg of MNPs embedded in a polystyrene matrix (MNP/PSM) capped with polyethylene oxide, with an average diameter of 100 nm. A temperature hike from 27 °C to 52 °C was observed within a timeframe of 30 min. This phenomenon was further studied by using Si/MNP/PSM and polyacrylic acid-capped MNPs. A magnetic field value of 4.5 kA/m with 13.56 MHz increased the temperature over a period of 35 min [160,161]. These reports showed that surface functionalisation has a significant effect on the heating temperature and the magnetic field.

Agglomeration and intracellular immobilisation affect the heating ability of MNPs [134,155–162]. For example, the agglomeration of MNPs amplifies the heating factor. Engelmann et al. tested the heating efficiency of agglomerated MNP samples. The agglomeration amplified the heating factor by up to 22%, whereas immobilization of MNPs reduced the heating by 30%. Meanwhile, the binding of larger MNP agglomerates at the cellular scale decreased the heating capacity [165].

Iacovita et al. revealed that the size of MNPs plays a vital role in the heat dissipation factor for MHT treatment [166]. They synthesised MNPs with sizes of ~34 and ~270 nm via the polyol method using PEG and EG, respectively. Upon the application of 355 kHz AMF with an amplitude of 65 kAm<sup>-1</sup>, they obtained SAR saturation values of ~1400 and 400 Wg<sup>-1</sup>. These results showed that small MNPs are better candidates than large MNPs for MHT application due to big SAR values.

In MHT, spherical MNPs are normally used due the good heat capacity. However, this capacity is still not efficient enough to reach the optimal therapeutic heat efficiency. MNCs provide better SAR values than their spherical counterpart because of their enhanced chainlike particle formation and

surface anisotropy. In addition, 1D magnetite nanostructures (MNRs) constitute a novel approach in MHT due to their improved blood circulation period, larger surface area, and longer retention at cancer site than their cubical and spherical counterparts. Das et al. demonstrated highly crystalline MNRs with high SAR values of up to  $862 \text{ Wg}^{-1}$  under 800 Oe of AC field. The high values were due to the rapid alignment of the MNRs to the applied AC field, thus increasing the SAR values. This finding paved a new path for advanced MHT [167].

Rong Fu et al. recently investigated the effect of inter-particle dipole interactions on the hyperthermia heating of densely packed MNP colloidal clusters at low field intensity. They assembled oleic acid-modified MNPs into compact clusters through the emulsion droplet solvent evaporation approach, where surfactant was used to stabilise the clusters in water. The shape anisotropy of the size of the clusters was influenced by the heating efficiency. Small clusters were able to improvise the shape anisotropy of the clusters, where the heating was enhanced through the dipole interactions. The reduction in shape anisotropy at large-sized clusters (clusters became more spherical in shape) varied the dipole interactions, thus impairing the heating efficiency. Thus, MNPs with higher magnetic anisotropy must be tuned to enhance the heating, which is essential for MHT [168].

Based on all the recent studies conducted, small, agglomerated MNPs with proper surface modifications, high saturation magnetisation values, and superparamagnetic properties constitute the best candidate for MHT.

## 5.2. In Vitro Applications

In vitro application is another type of surface-modified MNP application. In vitro diagnostic products are currently available in the market [13]. In this section, the two most common in vitro applications were discussed, i.e., bioseparation and biosensors.

### 5.2.1. Bioseparation

Bioseparation is a crucial type of in vitro antibody, cell, DNA, enzyme, gene, bacterial and viral separation, in which MNPs were successfully applied [169–171]. Compared with the traditional column affinity chromatography, magnetic separation possesses several advantages in terms of efficiency in retrieving or localising with a common magnet and cost. As in other applications, surface-modified MNPs with proper intermediates are normally used for separation enhancement. For surface functionalisation, ligands, polymers and surfactants are used to introduce functional groups (e.g.,  $-\text{COOH}$ ,  $-\text{NH}_2$ ,  $-\text{OH}$  and  $-\text{SH}$ ) on the target biomolecules via selective adsorption [13].

Chang et al. investigated the efficiency of separating bovine serum albumin (BSA) via functionalisation of hydrophobic pockets on the surface of  $\text{MNP@SiO}_2$  at different pH levels and alkyl groups. They observed efficient magnetic separation and achieved strong magnetic separation by controlling the alkyl chain length, pH levels, salt concentration and size of the hydrophobic pocket [172]. Chungang Wang and Joseph Irudayaraj reported a novel route to fabricate MNPs at the edges of Au nanorods by site-selective assembly method with various aspect ratios and synthesise multifunctional nanorods integrating magnetic and optical materials, resulting in alterable magnetic and plasmonic properties. They modified necklace-like magnetite-gold hybrid nanoparticles by using antibodies to enable efficient magnetic separation, thermal ablation, and optical detection of various pathogens in a single sample simultaneously [173]. Shao et al. applied the in-situ growth approach to synthesise three-component microspheres consisting of  $\text{SiO}_2$ -coated MNPs encapsulated with a layered double hydroxide nanoplatelet shell. The microspheres showed high saturation magnetisation values of  $36.8 \text{ emug}^{-1}$ , which portrayed superparamagnetism properties, and high magnetic separation of His-tagged protein from *Escherichia coli* lysate [174]. In addition, the high aspect ratios, adsorption properties, chemical composition, low toxicity, morphology, particle size and its distribution and stability of magnetic properties are utmost important in the application of MNP-based magnetic separation. Reza et al. discovered that the adhesions of BSA proteins for  $\text{MNP-SiO}_2$ ,  $\text{MNP-aminosilane}$

and MNP-SiO<sub>2</sub>-aminosilane arrays were 12.5%, 79.5%, and 145.75% more than those for bare MNPs, respectively [175].

MNPs are mostly preferred due to their superparamagnetic property. Moreover, due to their strong magnetic force, biomolecules could be transported easily towards targeted sites within the human body. Purification and isolation of different biomolecules, such as antibodies, DNAs, proteins, antigens, and nucleic acids could be performed at a highly purified percentage due to the strong magnetic force of MNPs.

### 5.2.2. Biosensors

In diagnostics, biosensing is an efficient platform for the detection of bacteria, biomolecules, cells, DNA, glucose, and viruses, with high sensitivity for diagnosing early diseases [134,176–178]. Biosensors are analytical devices utilised in the biomedical field. Their main function is converting biological, chemical, or biochemical response into electrical signals [144,179]. In addition, the surface functionalisation of MNPs is advantageous for the detection of molecular interactions; the large surface area of MNPs permits efficient functionalisation for targeted biomolecule interactions [13,134]. Xia Sun et al. determined carbofuran through composite immunosensors on the basis of Au nanoparticles by developing MNP-functionalised multiwalled CNT-chitosan (MNP-FCNT-chitosan) and BSA composite film. The immunosensors showed excellent stability, sensitivity, and accuracy in detecting carbofuran [180].

## 6. Conclusions and Perspectives

Recent progress in nanotechnology has displayed promising development and promptly advanced during the last decade on the basis of their adroitness in new diagnostic and therapeutic concepts in all aspects of nanomedicine. MNPs are simultaneously surface-modified and guided via an external magnetic field, thus delivering promising tools for several biological applications. MNPs could be modified so they could selectively accumulate at the tumour site and induce ‘targeted’ therapy, which conventional approaches could not do.

MNPs have multimodal functionality, with applications in therapeutic treatments and bioimaging diagnostics. In this review, MNPs were widely studied in terms of properties, synthesis methods and surface functionalisation for biomedical application efficiency in vivo and in vitro. For biomedical applications, MNPs could be efficiently synthesised through an array of approaches. In the synthesis of biocompatible MNPs, solubility in an aqueous solution should be primarily considered when deciding on the synthesis method to use. Common wet chemical methods, such as co-precipitation and solvothermal methods, fulfil this criterion. Although the co-precipitation method could directly synthesise water-soluble MNPs, poor size control and low crystallisation are the drawbacks. Most researchers prefer the solvothermal method when synthesising MNPs due to its ability to yield MNPs with high magnetic properties; well-controlled shapes and sizes; and high crystalline monodispersity, where tuning synthetic conditions play significant roles. The micro-/nano-emulsion method is used to functionalise MNPs with polymeric species for bioimaging, therapeutic moieties or drug loading. Surfactants are used to provide excellent control over shape and size of colloidal MNPs to be stabilised and possess superparamagnetism properties for applications in vivo and in vitro.

The main shortcoming of these MNPs is their hydrophobic surface chemistry that enables them to be soluble only in non-polar solvents, such as hexane and toluene. The surface chemistry of MNPs must be converted into hydrophilic to overcome this hindrance, in which organic and inorganic functionalisation were reported in this review. Surface functionalisation not only results in biocompatible surface chemistry for bioconjugation functions, but also provides additional physical properties such as optical resonance.

Previous reports on various biological applications, especially tumour theranostic applications in vivo and in vitro, indicated that enhancing the magnetic properties and SAR values of MNPs

improved the theranostic efficacy. However, the usage of MNPs in the early detection of tumours in conjunction with treatment is still in the developing phase.

**Author Contributions:** Conceptualization, D.D.B.; writing—original draft preparation, L.S.G.; writing—review and editing, D.D.B., R.M.Y., and M.A.M.; supervision, D.D.B. and M.A.M.; funding acquisition, D.D.B. and M.A.M. All authors have read and agreed to the published version of the manuscript.

**Funding:** The authors acknowledge the Ministry of Education for financial support under the Fundamental Research Grant Scheme FRGS/1/2018/STG07/UKM/02/15 and Universiti Kebangsaan Malaysia under Grant GUP-2019-072.

**Acknowledgments:** We acknowledge the administrative support given by Institute of Microengineering and Nanoelectronics (IMEN), UKM while doing this research. Special thanks to the open access journal publishers, which include IOP publishing for Figure 1, HALL archive for Figure 5, and the Royal Society publishing for Figure 11 for allowing us to re-use their figures.

**Conflicts of Interest:** The authors declare no conflict of interest.

## References

1. Sukumaran, S.; Neelakandan, M.S.; Shaji, N.; Prasad, P.; Yadunath, V.K. Magnetic Nanoparticles: Synthesis and Potential Biological Applications. *JSM Nanotechnol. Nanomed.* **2018**, *6*, 1068.
2. Kandasamy, G.; Maity, D. Recent advances in superparamagnetic iron oxide nanoparticles (SPIONs) for in vitro and in vivo cancer nanotheranostics. *Int. J. Pharm.* **2015**, *496*, 191–218. [[CrossRef](#)] [[PubMed](#)]
3. McNamara, K.; Tofail, S.A.M. Nanoparticles in biomedical applications. *Adv. Phys.* **2017**, *2*, 54–88. [[CrossRef](#)]
4. Ghazanfari, M.R.; Kashefi, M.; Shams, S.F.; Jaafari, M.R. Perspective of Fe<sub>3</sub>O<sub>4</sub> Nanoparticles Role in Biomedical Applications. *Biochem. Res. Int.* **2016**, *2016*, 1–32. [[CrossRef](#)]
5. Bhuiyan, M.T.H.; Chowdhury, M.N.; Parvin, M.S. Potential Nanomaterials and their Applications in Modern Medicine: An Overview. *ARC J. Cancer Sci.* **2016**, *2*, 25–33.
6. Chen, Y.-T.; Kolhatkar, A.G.; Zenasni, O.; Xu, S.; Lee, T.R. Biosensing Using Magnetic Particle Detection Techniques. *Sensors* **2017**, *17*, 2300. [[CrossRef](#)] [[PubMed](#)]
7. Chen, Y.; Ding, X.; Zhang, Y.; Natalia, A.; Sun, X.; Wang, Z.; Shao, H. Design and synthesis of magnetic nanoparticles for biomedical diagnostics. *Quant. Imaging Med. Surg.* **2018**, *8*, 957–970. [[CrossRef](#)] [[PubMed](#)]
8. McNamara, K.; Tofail, S.A. Nanosystems: The use of nanoalloys, metallic, bimetallic, and magnetic nanoparticles in biomedical applications. *Phys. Chem. Chem. Phys.* **2015**, *17*, 27981–27995. [[CrossRef](#)] [[PubMed](#)]
9. Liu, Y.; Zhu, W.; Wu, D.; Wei, Q. Electrochemical determination of dopamine in the presence of uric acid using palladium-loaded mesoporous Fe<sub>3</sub>O<sub>4</sub> nanoparticles. *Measurement* **2015**, *60*, 1–5. [[CrossRef](#)]
10. Sheng-Nan, S.; Chao, W.; Zan-Zan, Z.; Yang-Long, H.; Venkatraman, S.S.; Zhi-Chuan, X. Magnetic iron oxide nanoparticles: Synthesis and surface coating techniques for biomedical applications. *Chin. Phys. B* **2014**, *23*, 037503.
11. Xu, J.-K.; Zhang, F.-F.; Sun, J.-J.; Sheng, J.; Wang, F.; Sun, M. Bio and Nanomaterials Based on Fe<sub>3</sub>O<sub>4</sub>. *Molecules* **2014**, *19*, 21506–21528. [[CrossRef](#)] [[PubMed](#)]
12. Blaney, L. Magnetite (Fe<sub>3</sub>O<sub>4</sub>): Properties, Synthesis, and Applications. *Lehigh Univ. Lehigh Preserv.* **2007**, *15*, 5.
13. Wu, W.; Wu, Z.; Yu, T.; Jiang, C.Z.; Kim, W.-S. Recent progress on magnetic iron oxide nanoparticles: Synthesis, surface functional strategies and biomedical applications. *Sci. Technol. Adv. Mater.* **2015**, *16*, 023501. [[CrossRef](#)] [[PubMed](#)]
14. Schlegel, A.; Alvarado, S.F.; Wachter, P. Optical properties of magnetite (Fe<sub>3</sub>O<sub>4</sub>). *J. Phys. C Solid State Phys.* **1979**, *12*, 1157–1164. [[CrossRef](#)]
15. Cornell, R.M.; Schwertmann, U. *The Iron Oxides: Structure, Properties, Reactions, Occurrence and Uses*; VCH: Weinheim, Germany, 1996; pp. 6, 32, 119.
16. Ju, S.; Cai, T.; Lu, H.-S.; Gong, C.-D. Pressure-Induced Crystal Structure and Spin-State Transitions in Magnetite (Fe<sub>3</sub>O<sub>4</sub>). *J. Am. Chem. Soc.* **2012**, *134*, 13780–13786. [[CrossRef](#)] [[PubMed](#)]
17. Sun, S.; Zeng, H. Size-Controlled Synthesis of Magnetite Nanoparticles. *J. Am. Chem. Soc.* **2002**, *124*, 8204–8205. [[CrossRef](#)] [[PubMed](#)]

18. Martinez, G.; Malumbres, A.; Mallada, R.; Hueso, J.L.; Irusta, S.; Bomati-Miguel, O.; Santamaria, J. Use of a polyol liquid collection medium to obtain ultrasmall magnetic nanoparticles by laser pyrolysis. *Nanotechnology* **2012**, *23*, 425605. [[CrossRef](#)]
19. Bohra, M.; Agarwal, N.; Singh, V. A Short Review on Verwey Transition in Nanostructured Fe<sub>3</sub>O<sub>4</sub> Materials. *J. Nanomater.* **2019**, *2019*, 1–18. [[CrossRef](#)]
20. Liu, H.; Di Valentin, C. Band Gap in Magnetite above Verwey Temperature Induced by Symmetry Breaking. *J. Phys. Chem. C* **2017**, *121*, 25736–25742. [[CrossRef](#)]
21. Wright, J.P.; Attfield, J.P.; Radaelli, P.G. Charge ordered structure of magnetite Fe<sub>3</sub>O<sub>4</sub> below the Verwey transition. *Phys. Rev. B* **2002**, *66*, 214422. [[CrossRef](#)]
22. Tanwar, S.; Awana, V.P.S.; Singh, S.P.; Pasricha, R. Magnetic Field Dependence of Blocking Temperature in Oleic Acid Functionalized Iron Oxide Nanoparticles. *J. Supercond. Nov. Magn.* **2012**, *25*, 2041–2045. [[CrossRef](#)]
23. Saragi, T.; Sinaga, H.D.; Rahmi, F.; Pramesti, G.A.; Sugiarto, A.; Therigan, A.; Syakir, N.; Hidayat, S. Risdiana Blocking Temperature of Magnetite Nanoparticles Fe<sub>3</sub>O<sub>4</sub> Encapsulated Silicon Dioxide SiO<sub>2</sub>. *Key Eng. Mater.* **2020**, *855*, 172–176. [[CrossRef](#)]
24. Rumpf, K.; Granitzer, P.; Morales, M.D.P.; Poelt, P.; Reissner, M. Variable blocking temperature of a porous silicon/Fe<sub>3</sub>O<sub>4</sub> composite due to different interactions of the magnetic nanoparticles. *Nanoscale Res. Lett.* **2012**, *7*, 445. [[CrossRef](#)] [[PubMed](#)]
25. Majewski, P.; Thierry, B. Functionalized Magnetite Nanoparticles—Synthesis, Properties, and Bio-Applications. *Crit. Rev. Solid State Mater. Sci.* **2007**, *32*, 203–215. [[CrossRef](#)]
26. Moaca, E.-A.; Coricovac, D.E.; Şoica, C.; Pinzaru, I.A.; Păcurariu, C.; Dehelean, C. Preclinical Aspects on Magnetic Iron Oxide Nanoparticles and Their Interventions as Anticancer Agents: Eucleation, Apoptosis and Other Mechanism. In *Iron Ores and Iron Oxide Materials*; IntechOpen: London, UK, 2018.
27. Wallyn, J.; Anton, N.; Vandamme, T.F. Synthesis, Principles, and Properties of Magnetite Nanoparticles for In Vivo Imaging Applications—A Review. *Pharmaceutics* **2019**, *11*, 601. [[CrossRef](#)]
28. Thapa, D.; Palkar, V.; Kurup, M.; Malik, S. Properties of magnetite nanoparticles synthesized through a novel chemical route. *Mater. Lett.* **2004**, *58*, 2692–2694. [[CrossRef](#)]
29. Unni, M.; Uhl, A.M.; Savliwala, S.; Savitzky, B.H.; Dhavalikar, R.; Garraud, N.; Arnold, D.P.; Kourkoutis, L.F.; Andrew, J.S.; Rinaldi, C. Thermal Decomposition Synthesis of Iron Oxide Nanoparticles with Diminished Magnetic Dead Layer by Controlled Addition of Oxygen. *ACS Nano* **2017**, *11*, 2284–2303. [[CrossRef](#)]
30. Muscas, G.; Singh, G.; Glomm, W.R.; Mathieu, R.; Kumar, P.A.; Concas, G.; Agostinelli, E.; Peddis, D. Tuning the Size and Shape of Oxide Nanoparticles by Controlling Oxygen Content in the Reaction Environment: Morphological Analysis by Aspect Maps. *Chem. Mater.* **2015**, *27*, 1982–1990. [[CrossRef](#)]
31. Daoush, W.M. Co-Precipitation and Magnetic Properties of Magnetite Nanoparticles for Potential Biomedical Applications. *J. Nanomed. Res.* **2017**, *5*, 1–6. [[CrossRef](#)]
32. Alvarado, S.; Erbudak, M.; Munz, P. Final state effects in the 3d-photoelectron spectrum of Fe<sub>3</sub>O<sub>4</sub> and comparison with FeO. *Phys. B C* **1977**, *86*, 1188–1190. [[CrossRef](#)]
33. Zhang, X.X.; Schoenes, J.; Reim, W.; Wachter, P. Evidence for 3dn to 3dn-14s transitions in magnetite and in lithium and magnesium ferrites. *J. Phys. C Solid State Phys.* **1983**, *16*, 6055. [[CrossRef](#)]
34. Fontijn, W.W.; Van Der Zaag, P.J.; Devillers, M.A.C.; Brabers, V.A.M.; Metselaar, R.R. Optical and magneto-optical polar Kerr spectra of Fe<sub>3</sub>O<sub>4</sub> and Mg<sup>2+</sup>- or Al<sup>3+</sup>-substituted Fe<sub>3</sub>O<sub>4</sub>. *Phys. Rev. B* **1997**, *56*, 5432–5442. [[CrossRef](#)]
35. Schlegel, A.; Wächter, P. Optical properties of magnetite (Fe<sub>3</sub>O<sub>4</sub>) in the infrared. *J. Phys. Colloq.* **1980**, *41*, C5–C19. [[CrossRef](#)]
36. Shi, D.; Sadat, M.E.; Dunn, A.W.; Mast, D.B. Photo-fluorescent and magnetic properties of iron oxide nanoparticles for biomedical applications. *Nanoscale* **2015**, *7*, 8209–8232. [[CrossRef](#)] [[PubMed](#)]
37. Boxall, C.; Kelsall, G.; Zhang, Z. Photoelectrophoresis of colloidal iron oxides. Part 2.—Magnetite (Fe<sub>3</sub>O<sub>4</sub>). *J. Chem. Soc. Faraday Trans.* **1996**, *92*, 791–802. [[CrossRef](#)]
38. Fontijn, W.W.; Van Der Zaag, P.J.; Feiner, L.F.; Metselaar, R.R.; Devillers, M.A.C. A consistent interpretation of the magneto-optical spectra of spinel type ferrites (invited). *J. Appl. Phys.* **1999**, *85*, 5100–5105. [[CrossRef](#)]
39. Antonov, V.N.; Harmon, B.N.; Antropov, V.P.; Perlov, A.Y.; Yaresko, A.N. Electronic structure and magneto-optical Kerr effect of Fe<sub>3</sub>O<sub>4</sub> and Mg<sup>2+</sup>- or Al<sup>3+</sup>-substituted Fe<sub>3</sub>O<sub>4</sub>. *Phys. Rev. B* **2001**, *64*, 134410. [[CrossRef](#)]

40. Park, S.K.; Ishikawa, T.; Tokura, Y. Charge-gap formation upon the Verwey transition in Fe<sub>3</sub>O<sub>4</sub>. *Phys. Rev. B* **1998**, *58*, 3717–3720. [[CrossRef](#)]
41. Pan, P.; Lin, Y.; Gan, Z.X.; Luo, X.; Zhou, W.; Zhang, N. Magnetic field enhanced photothermal effect of Fe<sub>3</sub>O<sub>4</sub> nanoparticles. *J. Appl. Phys.* **2018**, *123*, 115115. [[CrossRef](#)]
42. Cornell, R.M.; Schwertmann, U. Chapter 2—Crystal structure. In *The Iron Oxides: Structure, Properties, Reactions, Occurrences and Uses*, 2nd ed.; Wiley-VCH Verlag GmbH & Co. KGaA: Weinheim, Germany, 2003; 9p.
43. Chicot, D.; Mendoza, J.; Zaoui, A.; Louis, G.; Lepingle, V.; Roudet, F.; Lesage, J. Mechanical properties of magnetite (Fe<sub>3</sub>O<sub>4</sub>), hematite (alpha-Fe<sub>2</sub>O<sub>3</sub>) and goethite (alpha-FeO center dot OH) by instrumented indentation and molecular dynamics analysis. *Mater. Chem. Phys.* **2011**, *129*, 862–870. [[CrossRef](#)]
44. Oolman, K.B.; Kattel, S.; Rice, K.P.; Rice, W.D. Magneto-Optical Properties of Iron Oxide Nanoparticles for Use in Medical Imaging. PhD Thesis, University of Wyoming, Laramie, Wyoming, 2017.
45. Yusoff, A.H.; Salimi, M.N.; Jamlos, M.F. A review: Synthetic strategy control of magnetite nanoparticles production. *Adv. Nano Res.* **2018**, *6*, 1.
46. Massart, R. Preparation of aqueous magnetic liquids in alkaline and acidic media. *IEEE Trans. Magn.* **1981**, *17*, 1247–1248. [[CrossRef](#)]
47. Baumgartner, J.; Dey, A.A.; Bomans, P.H.H.; Le Coadou, C.; Fratzl, P.; Sommerdijk, N.A.J.M.; Faivre, D. Nucleation and growth of magnetite from solution. *Nat. Mater.* **2013**, *12*, 310–314. [[CrossRef](#)] [[PubMed](#)]
48. Thanh, N.T.K.; MacLean, N.; Mahiddine, S. Mechanisms of Nucleation and Growth of Nanoparticles in Solution. *Chem. Rev.* **2014**, *114*, 7610–7630. [[CrossRef](#)] [[PubMed](#)]
49. Campbell, J. Magnetite/Silica Core-Shell Nanoparticles for HER-2 Targeted Magnetic Resonance Imaging of Breast Tumours. Ph.D. Thesis, Applied Sciences, RMIT University, Melbourne, Australia, 2013.
50. Davoudi, Z.; Akbarzadeh, A.; Rahmatiyamchi, M.; Movassaghpour, A.A.; Alipour, M.; Nejati-Koshki, K.; Sadeghi, Z.; Dariushnejad, H.; Zarghami, N. Molecular Target Therapy of AKT and NF-κB Signaling Pathways and Multidrug Resistance by Specific Cell Penetrating Inhibitor Peptides in HL-60 Cells. *Asian Pac. J. Cancer Prev.* **2014**, *15*, 4353–4358. [[CrossRef](#)] [[PubMed](#)]
51. Majidi, S.; Sehrig, F.Z.; Farkhani, S.M.; Goloujeh, M.S.; Saghati, S. Current methods for synthesis of magnetic nanoparticles. *Artif. Cells Nanomed. Biotechnol.* **2014**, *44*, 722–734. [[CrossRef](#)] [[PubMed](#)]
52. Govan, J.; Gun'Ko, Y.K. Recent Advances in the Application of Magnetic Nanoparticles as a Support for Homogeneous Catalysts. *Nanomaterials* **2014**, *4*, 222–241. [[CrossRef](#)]
53. Blanco-Andujar, C.; Ortega, D.; Pankhurst, Q.A.; Thanh, N.T.K. Elucidating the morphological and structural evolution of iron oxide nanoparticles formed by sodium carbonate in aqueous medium. *J. Mater. Chem.* **2012**, *22*, 12498–12506. [[CrossRef](#)]
54. Wu, S.; Sun, A.; Zhai, F.; Wang, J.; Xu, W.; Zhang, Q.; Volinsky, A.A. Fe<sub>3</sub>O<sub>4</sub> magnetic nanoparticles synthesis from tailings by ultrasonic chemical co-precipitation. *Mater. Lett.* **2011**, *65*, 1882–1884. [[CrossRef](#)]
55. Pereira, C.; Pereira, A.M.; Fernandes, C.; Rocha, M.; Mendes, R.; Fernández-García, M.P.; Guedes, A.; Tavares, P.B.; Grenèche, J.-M.; Araújo, J.P.; et al. Superparamagnetic MFe<sub>2</sub>O<sub>4</sub> (M = Fe, Co, Mn) Nanoparticles: Tuning the Particle Size and Magnetic Properties through a Novel One-Step Coprecipitation Route. *Chem. Mater.* **2012**, *24*, 1496–1504. [[CrossRef](#)]
56. Torrisi, V.; Graillot, A.; Vitorazi, L.; Crouzet, Q.; Marletta, G.; Loubat, C.; Berret, J.-F. Preventing Corona Effects: Multiphosponic Acid Poly(ethylene glycol) Copolymers for Stable Stealth Iron Oxide Nanoparticles. *Biomacromolecules* **2014**, *15*, 3171–3179. [[CrossRef](#)] [[PubMed](#)]
57. Wroblewski, C.; Volford, T.; Martos, B.; Samoluk, J.; Martos, P. High Yield Synthesis and Application of Magnetite Nanoparticles (Fe<sub>3</sub>O<sub>4</sub>). *Magnetochemistry* **2020**, *6*, 22. [[CrossRef](#)]
58. Faraji, M.; Yamini, Y.; Rezaee, M. Magnetic Nanoparticles: Synthesis, Stabilization, Functionalization, Characterization, and Applications. *J. Iran. Chem. Soc.* **2010**, *7*, 1–37. [[CrossRef](#)]
59. Sunny, V.; Kumar, D.S.; Yoshida, Y.; Makarewicz, M.; Tabis, W.; Anantharaman, M. Synthesis and properties of highly stable nickel/carbon core/shell nanostructures. *Carbon* **2010**, *48*, 1643–1651. [[CrossRef](#)]
60. Lin, X.; Ji, G.; Liu, Y.; Huang, Q.; Yang, Z.; Du, Y. Formation mechanism and magnetic properties of hollow Fe<sub>3</sub>O<sub>4</sub> nanospheres synthesized without any surfactant. *CrystrEngComm* **2012**, *14*, 8658–8663. [[CrossRef](#)]
61. Tian, Y.; Yu, B.; Li, X.; Li, K. Facile solvothermal synthesis of monodisperse Fe<sub>3</sub>O<sub>4</sub> nanocrystals with precise size control of one nanometre as potential MRI contrast agents. *J. Mater. Chem.* **2011**, *21*, 2476–2481. [[CrossRef](#)]

62. Stoia, M.; Păcurariu, C.; Istrate, R.; Nižňanský, D. Solvothermal synthesis of magnetic Fe x O y/C nanocomposites used as adsorbents for the removal of methylene blue from wastewater. *J. Therm. Anal. Calorim.* **2015**, *121*, 989–1001. [[CrossRef](#)]
63. Ahmadi, S.; Chia, C.-H.; Zakaria, S.; Saeedfar, K.; Asim, N. Synthesis of Fe<sub>3</sub>O<sub>4</sub> nanocrystals using hydrothermal approach. *J. Magn. Magn. Mater.* **2012**, *324*, 4147–4150. [[CrossRef](#)]
64. Wu, J.; Wang, L.; Lv, B.; Chen, J. Facile Fabrication of BCN Nanosheet-Encapsulated Nano-Iron as Highly Stable Fischer–Tropsch Synthesis Catalyst. *ACS Appl. Mater. Interfaces* **2017**, *9*, 14319–14327. [[CrossRef](#)]
65. Iacovita, C.; Stiuflu, R.; Radu, T.; Florea, A.; Stiuflu, G.; Dutu, A.G.; Mican, S.; Tetean, R.; Lucaciu, C.M. Polyethylene Glycol-Mediated Synthesis of Cubic Iron Oxide Nanoparticles with High Heating Power. *Nanoscale Res. Lett.* **2015**, *10*, 1–16. [[CrossRef](#)] [[PubMed](#)]
66. Aubery, C.; Solans, C. *New Trends on the Synthesis of Inorganic Nanoparticles Using Microemulsions as Confined Reaction Media*; IntechOpen: London, UK, 2012; pp. 195–220.
67. Lu, T.; Wang, J.; Yin, J.; Wang, A.; Wang, X.; Zhang, T. Surfactant effects on the microstructures of Fe<sub>3</sub>O<sub>4</sub> nanoparticles synthesized by microemulsion method. *Colloids Surf. A Physicochem. Eng. Asp.* **2013**, *436*, 675–683. [[CrossRef](#)]
68. Hasany, S.F.; Ahmed, I.; Rajan, J.; Rehman, A. Systematic Review of the Preparation Techniques of Iron Oxide Magnetic Nanoparticles. *Nanosci. Nanotechnol.* **2013**, *2*, 148–158. [[CrossRef](#)]
69. Xu, H.; Zeiger, B.W.; Suslick, K.S. Sonochemical synthesis of nanomaterials. *Chem. Soc. Rev.* **2013**, *42*, 2555–2567. [[CrossRef](#)] [[PubMed](#)]
70. Dolores, R.; Raquel, S.; Adianez, G.-L. Sonochemical synthesis of iron oxide nanoparticles loaded with folate and cisplatin: Effect of ultrasonic frequency. *Ultrason. Sonochem.* **2015**, *23*, 391–398. [[CrossRef](#)] [[PubMed](#)]
71. Theerdhala, S.; Bahadur, D.; Vitta, S.; Perkas, N.; Zhong, Z.; Gedanken, A. Sonochemical stabilization of ultrafine colloidal biocompatible magnetite nanoparticles using amino acid, l-arginine, for possible bio applications. *Ultrason. Sonochem.* **2010**, *17*, 730–737. [[CrossRef](#)] [[PubMed](#)]
72. Lu, T.; Guo, J.; Dong, J.; Cui, Z.; Lu, T.; Zhu, C.; Zhang, D.; Ma, J. Sonochemical fabrication of Fe<sub>3</sub>O<sub>4</sub> nanoparticles on reduced graphene oxide for biosensors. *Ultrason. Sonochem.* **2013**, *20*, 872–880.
73. Teo, B.M.; Chen, F.; Hatton, T.A.; Grieser, F.; AshokKumar, M. Novel One-Pot Synthesis of Magnetite Latex Nanoparticles by Ultrasound Irradiation. *Langmuir* **2009**, *25*, 2593–2595. [[CrossRef](#)] [[PubMed](#)]
74. Yew, Y.P.; Shameli, K.; Miyake, M.; Khairudin, N.B.B.A.; Mohamad, S.E.B.; Naiki, T.; Lee, K.X. Green biosynthesis of superparamagnetic magnetite Fe<sub>3</sub>O<sub>4</sub> nanoparticles and biomedical applications in targeted anticancer drug delivery system: A review. *Arab. J. Chem.* **2020**, *13*, 2287–2308. [[CrossRef](#)]
75. Lukman, A.I.; Gong, B.; Marjo, C.E.; Roessner, U.; Harris, A.T. Facile synthesis, stabilization, and anti-bacterial performance of discrete Ag nanoparticles using *Medicago sativa* seed exudates. *J. Colloid Interface Sci.* **2011**, *353*, 433–444. [[CrossRef](#)]
76. Shameli, K.; Ahmad, B.M.; Shabanzadeh, P.; Zamanian, A.; Sangpour, P.; Abdollahi, Y.; Mohsen, Z. Green biosynthesis of silver nanoparticles using *Curcuma longa* tuber powder. *Int. J. Nanomed.* **2012**, *7*, 5603–5610. [[CrossRef](#)] [[PubMed](#)]
77. Černík, M.; Padil, V.V.T. Green synthesis of copper oxide nanoparticles using gum karaya as a biotemplate and their antibacterial application. *Int. J. Nanomed.* **2013**, *8*, 889–898. [[CrossRef](#)] [[PubMed](#)]
78. Pourhassan-Moghaddam, M.; Zarghami, N.; Mohsenifar, A.; Rahmati-Yamchi, M.; Gholizadeh, D.; Akbarzadeh, A.; Nejati-Koshki, K. Watercress-based gold nanoparticles: Biosynthesis, mechanism of formation and study of their biocompatibility in vitro. *Micro Nano Lett.* **2014**, *9*, 345–350. [[CrossRef](#)]
79. Abbasi, E.; Milani, M.; Fekri Aval, S.; Kouhi, M.; Akbarzadeh, A.; Tayefi Nasrabadi, H. Silver nanoparticles: Synthesis, properties, bio-applications and limitations. *Crit. Rev. Microbiol.* **2014**, *1*, 1. [[CrossRef](#)] [[PubMed](#)]
80. Mukherjee, A. *Biomimetics: Learning from Nature*; BoD—Books on Demand: Norderstedt, Germany, 2010.
81. Pandey, S.; Oza, G.; Mewada, A.; Sharon, M. Green synthesis of highly stable gold nanoparticles using *Momordica charantia* as nano fabricator. *Arch. Appl. Sci. Res.* **2012**, *4*, 1135–1141.
82. Awwad, A.M.; Salem, N.M. A Green and Facile Approach for Synthesis of Magnetite Nanoparticles. *Nanosci. Nanotechnol.* **2013**, *2*, 208–213. [[CrossRef](#)]
83. Sundaram, P.A.; Augustine, R.; Kannan, M. Extracellular biosynthesis of iron oxide nanoparticles by *Bacillus subtilis* strains isolated from rhizosphere soil. *Biotechnol. Bioprocess Eng.* **2012**, *17*, 835–840. [[CrossRef](#)]
84. Eatemadi, A.; Daraee, H.; Zarghami, N.; Yar, H.M.; Akbarzadeh, A. Nanofiber: Synthesis and biomedical applications. *Artif. Cells Nanomed. Biotechnol.* **2014**, *44*, 111–121. [[CrossRef](#)]

85. Hosseininasab, S.; Pashaei-Asl, R.; Khandaghi, A.A.; Nasrabadi, H.T.; Nejati-Koshki, K.; Akbarzadeh, A.; Joo, S.W.; Hanifehpour, Y.; Davaran, S. Retracted: Synthesis, Characterization, and In vitro Studies of PLGA-PEG Nanoparticles for Oral Insulin Delivery. *Chem. Biol. Drug Des.* **2014**, *84*, 307–315. [[CrossRef](#)]
86. Nurbas, M.; Ghorbanpoor, H.; Avci, H. An eco-friendly approach to synthesis and characterization of magnetite (Fe<sub>3</sub>O<sub>4</sub>) nanoparticles using *Platanus orientalis* L. leaf extract. *Dig. J. Nanomater. Biostructures (DJNB)* **2017**, *12*, 993–1000.
87. Manteghi, F.; Omidvari, A.; Sohrabi, B.; Afra, Y. A Herbal Extract for the Synthesis of Magnetite Nanoparticles. In Proceedings of the 18th International Electronic Conference on Synthetic Organic Chemistry, 1–11 November 2014; Available online: <https://sciforum.net/conference/ecsoc-18> (accessed on 24 November 2020).
88. Yew, Y.P.; Shameli, K.; Miyake, M.; Kuwano, N.; Khairudin, N.B.B.A.; Mohamad, S.E.B.; Lee, K.X. Green Synthesis of Magnetite (Fe<sub>3</sub>O<sub>4</sub>) Nanoparticles Using Seaweed (*Kappaphycus alvarezii*) Extract. *Nanoscale Res. Lett.* **2016**, *11*, 1–7. [[CrossRef](#)]
89. Rasouli, E.; Basirun, W.J.; Rezayi, M.; Shameli, K.; Nourmohammadi, E.; Khandanlou, R.; Izadiyan, Z.; Sarkarizi, H.K. Ultrasmall superparamagnetic Fe<sub>3</sub>O<sub>4</sub> nanoparticles: Honey-based green and facile synthesis and in vitro viability assay. *Int. J. Nanomed.* **2018**, *13*, 6903–6911. [[CrossRef](#)] [[PubMed](#)]
90. Temelie, M.; Popescu, R.C.; Cocioaba, D.; Vasile, B.S.; Savu, D. Biocompatibility study of magnetite nanoparticle synthesized using a green method. *Rom. J. Phys.* **2018**, *63*, 703–716.
91. Mosayebi, J.; Kiyasatfar, M.; Laurent, S. Synthesis, Functionalization, and Design of Magnetic Nanoparticles for Theranostic Applications. *Adv. Health Mater.* **2017**, *6*, 1700306. [[CrossRef](#)] [[PubMed](#)]
92. Bohara, R.A.; Thorat, N.D.; Pawar, S.H. Role of functionalization: Strategies to explore potential nano-bio applications of magnetic nanoparticles. *RSC Adv.* **2016**, *6*, 43989–44012. [[CrossRef](#)]
93. Sundaresan, V.; Menon, J.U.; Rahimi, M.; Nguyen, K.T.; Wadajkar, A.S. Dual-responsive polymer-coated iron oxide nanoparticles for drug delivery and imaging applications. *Int. J. Pharm.* **2014**, *466*, 1–7. [[CrossRef](#)] [[PubMed](#)]
94. Wadajkar, A.S.; Menon, J.U.; Tsai, Y.-S.; Gore, C.; Dobin, T.; Gandee, L.; Kangasniemi, K.; Takahashi, M.; Manandhar, B.; Ahn, J.-M.; et al. Prostate cancer-specific thermo-responsive polymer-coated iron oxide nanoparticles. *Biomaterials* **2013**, *34*, 3618–3625. [[CrossRef](#)] [[PubMed](#)]
95. Chen, L. Surface Functionalization and Bioconjugation of Nanoparticles for Biomedical Applications. Ph.D. Thesis, The University of Western Ontario, London, ON, Canada, 2014.
96. Vera, N.P.M.; Schmidt, R.; Langer, K.; Zlatev, I.; Wronski, R.; Auer, E.; Havas, D.; Windisch, M.; Von Briesen, H.; Wagner, S.; et al. Tracking of Magnetite Labeled Nanoparticles in the Rat Brain Using MRI. *PLoS ONE* **2014**, *9*, e92068.
97. Kloust, H.; Schmidtke, C.; Feld, A.; Schotten, T.; Eggers, R.; Fittschen, U.E.A.; Schulz, F.; Pösel, E.; Ostermann, J.; Bastús, N.G.; et al. In Situ Functionalization and PEO Coating of Iron Oxide Nanocrystals Using Seeded Emulsion Polymerization. *Langmuir* **2013**, *29*, 4915–4921. [[CrossRef](#)]
98. Li, L.; Jiang, W.; Luo, K.; Song, H.; Lan, F.; Wu, Y.; Gu, Z. Superparamagnetic Iron Oxide Nanoparticles as MRI contrast agents for Non-invasive Stem Cell Labeling and Tracking. *Theranostics* **2013**, *3*, 595–615. [[CrossRef](#)]
99. Shen, M.; Cai, H.; Wang, X.; Cao, X.; Li, K.; Wang, S.H.; Guo, R.; Zheng, L.; Zhang, G.; Shi, X. Facile one-pot preparation, surface functionalization, and toxicity assay of APTS-coated iron oxide nanoparticles. *Nanotechnology* **2012**, *23*, 105601. [[CrossRef](#)] [[PubMed](#)]
100. Dheyab, M.A.; Aziz, A.A.; Jameel, M.S.; Abu Noqta, O.; Khaniabadi, P.M.; Mehrdel, B. Simple rapid stabilization method through citric acid modification for magnetite nanoparticles. *Sci. Rep.* **2020**, *10*, 1–8. [[CrossRef](#)] [[PubMed](#)]
101. Smolensky, E.D.; Park, H.-Y.E.; Zhou, Y.; Rolla, G.A.; Marjańska, M.; Botta, M.; Pierre, V.C. Scaling laws at the nanosize: The effect of particle size and shape on the magnetism and relaxivity of iron oxide nanoparticle contrast agents. *J. Mater. Chem. B* **2013**, *1*, 2818–2828. [[CrossRef](#)] [[PubMed](#)]
102. Bae, J.; Lawrence, J.; Miesch, C.; Ribbe, A.; Li, W.; Emrick, T.; Zhu, J.; Hayward, R.C. Multifunctional Nanoparticle-Loaded Spherical and Wormlike Micelles Formed by Interfacial Instabilities. *Adv. Mater.* **2012**, *24*, 2735–2741. [[CrossRef](#)] [[PubMed](#)]
103. Gao, J.; Ran, X.; Shi, C.; Cheng, H.; Cheng, T.; Su, Y. One-step solvothermal synthesis of highly water-soluble, negatively charged superparamagnetic Fe<sub>3</sub>O<sub>4</sub> colloidal nanocrystal clusters. *Nanoscale* **2013**, *5*, 7026–7033. [[CrossRef](#)] [[PubMed](#)]

104. Ali, N.; Zhang, B.; Zhang, H.; Zaman, W.; Baoliang, W.; Zhang, Q. Key synthesis of magnetic Janus nanoparticles using a modified facile method. *Particuology* **2014**, *17*, 59–65. [[CrossRef](#)]
105. Cao, M.; Li, Z.; Wang, J.; Ge, W.; Yue, T.; Li, R.; Colvin, V.L.; Yu, W.W. Food related applications of magnetic iron oxide nanoparticles: Enzyme immobilization, protein purification, and food analysis. *Trends Food Sci. Technol.* **2012**, *27*, 47–56. [[CrossRef](#)]
106. Iwaki, Y.; Kawasaki, H.; Arakawa, R. Human serum albumin-modified Fe<sub>3</sub>O<sub>4</sub> magnetic nanoparticles for affinity-SALDI-MS of small-molecule drugs in biological liquids. *Anal. Sci.* **2012**, *28*, 893–900. [[CrossRef](#)]
107. Okuda, M.; Eloi, J.-C.; Jones, S.E.W.; Sarua, A.; Richardson, R.M.; Schwarzacher, W. Fe<sub>3</sub>O<sub>4</sub> nanoparticles: Protein-mediated crystalline magnetic superstructures. *Nanotechnology* **2012**, *23*, 415601. [[CrossRef](#)]
108. Marcelo, G.; Munozbonilla, A.; Rodriguezhernandez, J.; Fernandezgarcia, M. Hybrid materials achieved by polypeptide grafted magnetite nanoparticles through a dopamine biomimetic surface anchored initiator. *Polym. Chem.* **2013**, *4*, 558–567. [[CrossRef](#)]
109. Xie, J.; Wang, J.; Niu, G.; Huang, J.; Chen, K.; Li, X.; Chen, X. Human serum albumin coated iron oxide nanoparticles for efficient cell labeling. *Chem. Commun.* **2010**, *46*, 433–435. [[CrossRef](#)] [[PubMed](#)]
110. Bhattacharya, D.; Chakraborty, S.P.; Pramanik, A.; Baksi, A.; Roy, S.S.; Maiti, T.K.; Ghosh, S.K.; Pramanik, P. Detection of total count of Staphylococcus aureus using anti-toxin antibody labelled gold magnetite nanocomposites: A novel tool for capture, detection and bacterial separation. *J. Mater. Chem.* **2011**, *21*, 17273. [[CrossRef](#)]
111. Ye, Y.; Kuai, L.; Geng, B. A template-free route to a Fe<sub>3</sub>O<sub>4</sub>-Co<sub>3</sub>O<sub>4</sub> yolk-shell nanostructure as a noble-metal free electrocatalyst for ORR in alkaline media. *J. Mater. Chem.* **2012**, *22*, 19132–19138. [[CrossRef](#)]
112. Zhao, Y.; Zhang, W.; Lin, Y.; Du, D. 2013 The vital function of Fe<sub>3</sub>O<sub>4</sub>@Au nanocomposites for hydrolase biosensor design and its application in detection of methyl parathion. *Nanoscale* **2013**, *5*, 1121–1126. [[CrossRef](#)] [[PubMed](#)]
113. He, X.; Tana, L.; Chen, N.; Wu, X.; Ren, X.; Zhang, Y.; Meng, X.; Tang, F. Fe<sub>3</sub>O<sub>4</sub>-Au@mesoporous SiO<sub>2</sub> microspheres: An ideal artificial enzymatic cascade system. *Chem. Commun.* **2013**, *49*, 4643. [[CrossRef](#)] [[PubMed](#)]
114. Wang, D.-W.; Zhu, X.-M.; Lee, S.-F.; Chan, G.H.; Li, H.-W.; Kong, S.K.; Yu, J.C.; Cheng, C.H.K.; Wang, Y.-X.J.; Leung, K.C.-F. Folate-conjugated Fe<sub>3</sub>O<sub>4</sub>@SiO<sub>2</sub>@gold nanorods@mesoporous SiO<sub>2</sub> hybrid nanomaterial: A theranostic agent for magnetic resonance imaging and photothermal therapy. *J. Mater. Chem. B* **2013**, *1*, 2934–2942. [[CrossRef](#)]
115. Zhu, N.; Ji, H.; Yu, P.; Niu, J.; Farooq, M.U.; Akram, M.W.; Udego, I.O.; Li, H.; Niu, X. Surface Modification of Magnetic Iron Oxide Nanoparticles. *Nanomaterials* **2018**, *8*, 810. [[CrossRef](#)]
116. Zhu, Y.; Ikoma, T.; Hanagata, N.; Kaskel, S. Rattle-Type Fe<sub>3</sub>O<sub>4</sub>@SiO<sub>2</sub> Hollow Mesoporous Spheres as Carriers for Drug Delivery. *Small* **2010**, *6*, 471–478. [[CrossRef](#)]
117. Shao, J.; Xie, X.; Xi, Y.; Liu, X.; Yang, Y. Characterization of Fe<sub>3</sub>O<sub>4</sub>/SiO<sub>2</sub> composite core-shell nanoparticles synthesized in isopropanol medium. *Glass Phys. Chem.* **2013**, *39*, 329–335. [[CrossRef](#)]
118. Cao, Z.; Yang, L.; Ye, Q.; Cui, Q.; Qi, D.; Ziener, U. Transition-Metal Salt-Containing Silica Nanocapsules Elaborated via Salt-Induced Interfacial Deposition in Inverse Miniemulsions as Precursor to Functional Hollow Silica Particles. *Langmuir* **2013**, *29*, 6509–6518. [[CrossRef](#)]
119. Stöber, W.; Fink, A.; Bohn, E. Controlled growth of monodisperse silica spheres in the micron size range. *J. Colloid Interface Sci.* **1968**, *26*, 62–69. [[CrossRef](#)]
120. Wu, W.; Xiao, X.H.; Zhang, S.F.; Fan, L.X.; Peng, T.C.; Ren, F.; Jiang, C.Z. Facile fabrication of ultrafine hollow silica and magnetic hollow silica nanoparticles by a dualtemplating approach. *Nanoscale Res. Lett.* **2010**, *5*, 116. [[CrossRef](#)] [[PubMed](#)]
121. Pinho, S.L.C.; Laurent, S.; Rocha, J.; Roch, A.; Delville, M.-H.; Mornet, S.; Carlos, L.D.; Elst, L.V.; Muller, R.N.; Geraldes, C.F.G.C. Relaxometric Studies of  $\gamma$ -Fe<sub>2</sub>O<sub>3</sub>@SiO<sub>2</sub> Core Shell Nanoparticles: When the Coating Matters. *J. Phys. Chem. C* **2012**, *116*, 2285–2291. [[CrossRef](#)]
122. Park, J.-N.; Zhang, P.; Hu, Y.-S.; McFarland, E.W. Synthesis and characterization of sintering-resistant silica-encapsulated Fe<sub>3</sub>O<sub>4</sub> magnetic nanoparticles active for oxidation and chemical looping combustion. *Nanotechnology* **2010**, *21*, 225708. [[CrossRef](#)] [[PubMed](#)]
123. Ding, H.L.; Zhang, Y.; Wang, S.; Xu, J.M.; Xu, S.C.; Li, G.H. Fe<sub>3</sub>O<sub>4</sub>@SiO<sub>2</sub> Core/Shell Nanoparticles: The Silica Coating Regulations with a Single Core for Different Core Sizes and Shell Thicknesses. *Chem. Mater.* **2012**, *24*, 4572–4580. [[CrossRef](#)]

124. Bae, H.; Ahmad, T.; Rhee, I.; Chang, Y.; Jin, S.-U.; Hong, S. Carbon-coated iron oxide nanoparticles as contrast agents in magnetic resonance imaging. *Nanoscale Res. Lett.* **2012**, *7*, 44. [[CrossRef](#)] [[PubMed](#)]
125. Li, L.; Wang, T.; Zhang, L.; Su, Z.-M.; Wang, C.; Wang, R. Selected-Control Synthesis of Monodisperse Fe<sub>3</sub>O<sub>4</sub>@C Core-Shell Spheres, Chains, and Rings as High-Performance Anode Materials for Lithium-Ion Batteries. *Chem. A Eur. J.* **2012**, *18*, 11417–11422. [[CrossRef](#)]
126. Fan, X.; Jiao, G.; Zhao, W.; Jin, P.; Li, X. Magnetic Fe<sub>3</sub>O<sub>4</sub>—Graphene composites as targeted drug nanocarriers for pH-activated release. *Nanoscale* **2013**, *5*, 1143–1152. [[CrossRef](#)]
127. Li, X.; Huang, X.; Liu, D.; Wang, X.; Song, S.; Zhou, L.; Zhang, H. Synthesis of 3D hierarchical Fe<sub>3</sub>O<sub>4</sub>/graphene composites with high lithium storage capacity and for controlled drug delivery. *J. Phys. Chem. C* **2011**, *115*, 21567–21573. [[CrossRef](#)]
128. Cong, H.-P.; He, J.-J.; Lu, Y.; Yu, S.-H. Water-Soluble Magnetic-Functionalized Reduced Graphene Oxide Sheets: In situ Synthesis and Magnetic Resonance Imaging Applications. *Small* **2010**, *6*, 169–173. [[CrossRef](#)]
129. Chen, W.; Yi, P.; Zhang, Y.; Zhang, L.; Deng, Z.; Zhang, Z. Composites of Aminodextran-Coated Fe<sub>3</sub>O<sub>4</sub> Nanoparticles and Graphene Oxide for Cellular Magnetic Resonance Imaging. *ACS Appl. Mater. Interfaces* **2011**, *3*, 4085–4091. [[CrossRef](#)] [[PubMed](#)]
130. Zhu, Z.; Rezhdo, O.; Perrone, M.; Bao, Z.; Munir, A.; Wang, J.; Zhou, H.S.; Shao, J. Magnetite nanoparticles doped photoresist derived carbon as a suitable substratum for nerve cell culture. *Colloids Surf. B Biointerfaces* **2013**, *102*, 428–434. [[CrossRef](#)] [[PubMed](#)]
131. Mendes, R.G.; Koch, B.; Bachmatiuk, A.; El-Gendy, A.A.; Krupskaya, Y.; Springer, A.; Klingeler, R.; Schmidt, O.G.; Büchner, B.; Sanchez, S.; et al. Synthesis and toxicity characterization of carbon coated iron oxide nanoparticles with highly defined size distributions. *Biochim. Biophys. Acta (BBA) Gen. Subj.* **2014**, *1840*, 160–169. [[CrossRef](#)] [[PubMed](#)]
132. Bahari, A. Characteristics of Fe<sub>3</sub>O<sub>4</sub>, α-Fe<sub>2</sub>O<sub>3</sub>, and γ-Fe<sub>2</sub>O<sub>3</sub> Nanoparticles as Suitable Candidates in the Field of Nanomedicine. *J. Supercond. Nov. Magn.* **2017**, *30*, 2165–2174. [[CrossRef](#)]
133. Khan, K.; Rehman, S.; Rahman, H.U.; Khan, Q. Synthesis and application of magnetic nanoparticles. *Nanomagnetism* **2014**, *6*, 135–159.
134. Abdullh, N. Surface Functionalization of Magnetic Nanoparticles Towards Biomedical Applications. Master's Thesis, School of Mechanical, Materials, Mechatronic and Biomedical Engineering, University of Wollongong, Wollongong, Australia, 2018.
135. Sandler, S.E.; Fellows, B.D.; Mefford, O.T. Best Practices for Characterization of Magnetic Nanoparticles for Biomedical Applications. *Anal. Chem.* **2019**, *91*, 14159–14169. [[CrossRef](#)]
136. Nochehdehi, A.R.; Thomas, S.; Sadri, M.; Afghahi, S.S.S.; Hadavi, S.M. Iron Oxide Biomagnetic Nanoparticles (IO-BMNPs); Synthesis, Characterization and Biomedical Application—A Review. *J. Nanomed. Nanotechnol.* **2017**, *8*, 1–9.
137. Saifullah, S.; Ali, I.; Kawish, M.; El-Shabasy, R.M.; Chen, L.; El-Seedi, H.R. Surface functionalized magnetic nanoparticles for targeted cancer therapy and diagnosis. In *Metal Nanoparticles for Drug Delivery and Diagnostic Applications*; Elsevier: Amsterdam, The Netherlands, 2020; pp. 215–236.
138. Oltolina, F.; Peigneux, A.; Colangelo, D.; Clemente, N.; D'Urso, A.; Valente, G.; Iglesias, G.R.; Jiménez-Lopez, C.; Prat, M. Biomimetic Magnetite Nanoparticles as Targeted Drug Nanocarriers and Mediators of Hyperthermia in an Experimental Cancer Model. *Cancers* **2020**, *12*, 2564. [[CrossRef](#)]
139. Vuongaf, T.K.; Le, T.T.; Do, H.D.; Nguyen, X.T.; Vu, T.T.; Le, T.L.; Tran, L.D. PMAO-assisted thermal decomposition synthesis of high-stability ferrofluid based on magnetite nanoparticles for hyperthermia and MRI applications. *Mater. Chem. Phys.* **2020**, *245*, 122762. [[CrossRef](#)]
140. Estelrich, J.; Escribano, E.; Queralt, J.; Busquets, M.A. Iron Oxide Nanoparticles for Magnetically-Guided and Magnetically-Responsive Drug Delivery. *Int. J. Mol. Sci.* **2015**, *16*, 8070–8101. [[CrossRef](#)]
141. Malumbres, A.; Martínez, G.; Mallada, R.; Hueso, J.L.; Bomati-Miguel, O.; Santamaría, J. Continuous production of iron-based nanocrystals by laser pyrolysis. Effect of operating variables on size, composition and magnetic response. *Nanotechnology* **2013**, *24*, 325603. [[CrossRef](#)] [[PubMed](#)]
142. Eremin, A.V.; Gurentsov, E.V.; Mikheyeva, E.Y.; Musikhin, S.A. Binary iron-carbon nanoparticle synthesis in photolysis of Fe(CO)<sub>5</sub> with methane and acetylene. *J. Phys. Conf. Ser.* **2016**, *774*, 012127. [[CrossRef](#)]
143. Kang, J.; Kim, Y.; Kim, H.-M.; Hu, X.; Saito, N.; Choi, J.-H.; Lee, M.-H. In-situ one-step synthesis of carbon-encapsulated naked magnetic metal nanoparticles conducted without additional reductants and agents. *Sci. Rep.* **2016**, *6*, 38652. [[CrossRef](#)] [[PubMed](#)]

144. Vieira, A.P.M.; Arias, L.S.; Neto, F.N.D.S.; Kubo, A.M.; Lima, B.H.R.; De Camargo, E.R.; Pessan, J.P.; Delbem, A.C.B.; Monteiro, D.R. Antibiofilm effect of chlorhexidine-carrier nanosystem based on iron oxide magnetic nanoparticles and chitosan. *Colloids Surf. B Biointerfaces* **2019**, *174*, 224–231. [[CrossRef](#)]
145. Fikai, D.; Fikai, A.; Andronescu, E. Advances in Cancer Treatment: Role of Nanoparticles. In *Nanomaterials—Toxicity and Risk Assessment*; IntechOpen: London, UK, 2015; pp. 1–22.
146. Chen, F.-H.; Zhang, L.-M.; Chen, Q.-T.; Zhang, Y.; Zhang, Z.-J. Synthesis of a novel magnetic drug delivery system composed of doxorubicin-conjugated Fe<sub>3</sub>O<sub>4</sub> nanoparticle cores and a PEG-functionalized porous silica shell. *Chem. Commun.* **2010**, *46*, 8633–8635. [[CrossRef](#)] [[PubMed](#)]
147. Deng, H.; Lei, Z. Preparation and characterization of hollow Fe<sub>3</sub>O<sub>4</sub>/SiO<sub>2</sub>@PEG-PLA nanoparticles for drug delivery. *Compos. Part B Eng.* **2013**, *54*, 194–199. [[CrossRef](#)]
148. Joshi, H.M.; De, I.; Richter, F.; He, J.; Prasad, P.V.; Dravid, V.P. Effect of silica shell thickness of Fe<sub>3</sub>O<sub>4</sub>-SiO<sub>x</sub> core-shell nanostructures on MRI contrast. *J. Nanoparticle Res.* **2013**, *15*, 460. [[CrossRef](#)]
149. Mahmoud, W.E.; Bronstein, L.M.; Al-Hazmi, F.; Al-Noaiser, F.; Al-Ghamdi, A.A. Development of Fe/Fe<sub>3</sub>O<sub>4</sub> Core-Shell Nanocubes as a Promising Magnetic Resonance Imaging Contrast Agent. *Langmuir* **2013**, *29*, 13095–13101. [[CrossRef](#)]
150. Zeng, L.; Ren, W.; Xiang, L.; Zheng, J.; Chen, B.; Wu, A. Multifunctional Fe<sub>3</sub>O<sub>4</sub>-TiO<sub>2</sub> nanocomposites for magnetic resonance imaging and potential photodynamic therapy. *Nanoscale* **2013**, *5*, 2107. [[CrossRef](#)]
151. Smolensky, E.D.; Neary, M.C.; Zhou, Y.; Berquo, T.S.; Pierre, V.C. Fe<sub>3</sub>O<sub>4</sub>@organic@Au: Core-shell nanocomposites with high saturation magnetisation as magnetoplasmonic MRI contrast agents. *Chem. Commun.* **2011**, *47*, 2149–2151. [[CrossRef](#)]
152. Zhou, Y.-M.; Wang, H.-B.; Gong, M.; Sun, Z.; Cheng, K.; Kong, X.-K.; Guo, Z.; Chen, Q. Yolk-type Au@Fe<sub>3</sub>O<sub>4</sub>@C nanospheres for drug delivery, MRI and two-photon fluorescence imaging. *Dalton Trans.* **2013**, *42*, 9906–9913. [[CrossRef](#)] [[PubMed](#)]
153. Gonzalez-Rodriguez, R.; Granitzer, P.; Rumpf, K.; Coffey, J.L. New MRI contrast agents based on silicon nanotubes loaded with superparamagnetic iron oxide nanoparticles. *R. Soc. Open Sci.* **2018**, *5*, 180697. [[CrossRef](#)] [[PubMed](#)]
154. Ardelean, I.L.; Stoencea, L.B.N.; Fikai, D.; Fikai, A.; Trusca, R.; Vasile, B.S.; Nechifor, G.; Andronescu, E. Development of Stabilized Magnetite Nanoparticles for Medical Applications. *J. Nanomater.* **2017**, *2017*, 1–9. [[CrossRef](#)]
155. Moradiya, M.A.; Ladani, A.; Ladani, J.; Raiyani, C.; Markna, J.H. New Way to Treat Cancer: Magnetic Nanoparticle based Hyperthermia. *J. Chem. Sci. Eng.* **2019**, *2*, 58–60.
156. Estelrich, J.; Busquets, M.A. Iron Oxide Nanoparticles in Photothermal Therapy. *Molecules* **2018**, *23*, 1567. [[CrossRef](#)]
157. Nemala, H.B. Investigation of Temperature Dependent Magnetic Hyperthermia in Fe<sub>3</sub>O<sub>4</sub> Ferrofluids. Ph.D. Thesis, Wayne State University, Detroit, MI, USA, 2015.
158. Perigo, E.A.; Hemery, G.; Sandre, O.; Ortega, D.; Garaio, E.; Plazaola, F.; Teran, F.J. Fundamentals and advances in magnetic hyperthermia. *Appl. Phys. Rev.* **2015**, *2*, 041302. [[CrossRef](#)]
159. Martínez, F.P.; Simeonidis, K.; Makridis, A.; Angelakeris, M.; Iglesias, O.; Guardia, P.; Cabot, A.; Yedra, L.; Estradé, S.; Peiró, F.; et al. Learning from Nature to Improve the Heat Generation of Iron-Oxide Nanoparticles for Magnetic Hyperthermia Applications. *Sci. Rep.* **2013**, *3*, 1652. [[CrossRef](#)]
160. Sadat, M.; Patel, R.; Bud'ko, S.L.; Ewing, R.C.; Zhang, J.; Xu, H.; Mast, D.B.; Shi, D. Dipole-interaction mediated hyperthermia heating mechanism of nanostructured Fe<sub>3</sub>O<sub>4</sub> composites. *Mater. Lett.* **2014**, *129*, 57–60. [[CrossRef](#)]
161. Sadat, M.; Patel, R.; Sookoor, J.; Bud'ko, S.L.; Ewing, R.C.; Zhang, J.; Xu, H.; Wang, Y.; Pauletti, G.M.; Mast, D.B.; et al. Effect of spatial confinement on magnetic hyperthermia via dipolar interactions in Fe<sub>3</sub>O<sub>4</sub> nanoparticles for biomedical applications. *Mater. Sci. Eng. C* **2014**, *42*, 52–63. [[CrossRef](#)]
162. Surowiec, Z.; Miaskowski, A.; Budzyński, M. Investigation of magnetite Fe<sub>3</sub>O<sub>4</sub> nanoparticles for magnetic hyperthermia. *Nukleonika* **2017**, *62*, 183–186. [[CrossRef](#)]
163. Macías-Martínez, B.; Cortés, D.A.; Zugasti-Cruz, A.; Cruz-Ortíz, B.; Múzquiz-Ramos, E.M. Heating ability and hemolysis test of magnetite nanoparticles obtained by a simple co-precipitation method. *J. Appl. Res. Technol.* **2016**, *14*, 239–244. [[CrossRef](#)]

164. Hayashi, K.; Nakamura, M.; Miki, H.; Ozaki, S.; Abe, M.; Matsumoto, T.; Sakamoto, W.; Yogo, T.; Ishimura, K. Magnetically Responsive Smart Nanoparticles for Cancer Treatment with a Combination of Magnetic Hyperthermia and Remote-Control Drug Release. *Theranostics* **2014**, *4*, 834–844. [[CrossRef](#)] [[PubMed](#)]
165. Mues, B.; Buhl, E.M.; Baumann, M.; Schmitz-Rode, T.; Slabu, I. Agglomeration of magnetic nanoparticles and its effects on magnetic hyperthermia. *Curr. Dir. Biomed. Eng.* **2017**, *3*, 457–460.
166. Iacovita, C.; Florea, A.; Dudric, R.; Páll, E.; Moldovan, A.; Tetean, R.; Stiufiuc, R.; Lucaciu, C.M. Small versus Large Iron Oxide Magnetic Nanoparticles: Hyperthermia and Cell Uptake Properties. *Molecules* **2016**, *21*, 1357. [[CrossRef](#)] [[PubMed](#)]
167. Das, R.; Alonso, J.; Porshokouh, Z.N.; Kalappattil, V.; Torres, D.; Phan, M.-H.; Garaio, E.; García, J. Ángel; Llamazares, J.L.S.; Srikanth, H. Tunable High Aspect Ratio Iron Oxide Nanorods for Enhanced Hyperthermia. *J. Phys. Chem. C* **2016**, *120*, 10086–10093. [[CrossRef](#)]
168. Fu, R.; Yan, Y.; Roberts, C.; Liu, Z.; Chen, Y. The role of dipole interactions in hyperthermia heating colloidal clusters of densely-packed superparamagnetic nanoparticles. *Sci. Rep.* **2018**, *8*, 1–10. [[CrossRef](#)] [[PubMed](#)]
169. Fatima, H.; Kim, K.-S. Magnetic nanoparticles for bioseparation. *Korean J. Chem. Eng.* **2017**, *34*, 589–599. [[CrossRef](#)]
170. Sehrig, F.Z.; Majidi, S.; Nikzamir, N.; Nikzamir, N.; Nikzamir, M.; Akbarzadeh, A. Magnetic nanoparticles as potential candidates for biomedical and biological applications. *Artif. Cells Nanomed. Biotechnol.* **2015**, *44*, 1–10. [[CrossRef](#)]
171. Denison, M.I.J.; Raman, S.; Duraisamy, N.; Thangavelu, R.M.; Riyaz, S.U.M.; Gunasekaran, D.; Krishnan, K. Preparation, characterization and application of antibody-conjugated magnetic nanoparticles in the purification of begomovirus. *RSC Adv.* **2015**, *5*, 99820–99831. [[CrossRef](#)]
172. Chang, J.H.; Lee, J.; Jeong, Y.; Lee, J.H.; Kim, I.J.; Park, S.E. Hydrophobic partitioning approach to efficient protein separation with magnetic nanoparticles. *Anal. Biochem.* **2010**, *405*, 135–137. [[CrossRef](#)]
173. Wang, C.; Irudayaraj, J. Multifunctional Magnetic-Optical Nanoparticle Probes for Simultaneous Detection, Separation, and Thermal Ablation of Multiple Pathogens. *Small* **2010**, *6*, 283–289. [[CrossRef](#)] [[PubMed](#)]
174. Shao, M.; Ning, F.; Zhao, J.; Wei, M.; Evans, D.G.; Duan, X. Preparation of Fe<sub>3</sub>O<sub>4</sub>@SiO<sub>2</sub>@Layered Double Hydroxide Core-Shell Microspheres for Magnetic Separation of Proteins. *J. Am. Chem. Soc.* **2012**, *134*, 1071–1077. [[CrossRef](#)]
175. Reza, R.T.; Pérez, C.A.M.; Martínez, A.M.; Baques, D.B.; García-Casillas, P.E. Study of the Particle Size Effect on the Magnetic Separation of Bovine Serum Albumin (BSA). *Sens. Lett.* **2010**, *8*, 476–481. [[CrossRef](#)]
176. Hosu, O.; Tertis, M.; Cristea, C. Hosu Implication of Magnetic Nanoparticles in Cancer Detection, Screening and Treatment. *Magnetochemistry* **2019**, *5*, 55. [[CrossRef](#)]
177. Saylan, Y.; Erdem, Ö.; Ünal, S.; Denizli, A. An Alternative Medical Diagnosis Method: Biosensors for Virus Detection. *Biosensors* **2019**, *9*, 65. [[CrossRef](#)] [[PubMed](#)]
178. Vidic, J.; Manzano, M.; Chang, C.-M.; Jaffrezic-Renault, N. Advanced biosensors for detection of pathogens related to livestock and poultry. *Veter Res.* **2017**, *48*, 1–22. [[CrossRef](#)]
179. Mehrotra, P. Biosensors and their applications—A review. *J. Oral Biol. Craniofacial Res.* **2016**, *6*, 153–159. [[CrossRef](#)]
180. Sun, X.; Li, Q.; Wang, X.; Du, S. Amperometric Immunosensor Based on Gold Nanoparticles/Fe<sub>3</sub>O<sub>4</sub>-FCNTs-CS Composite Film Functionalized Interface for Carbofuran Detection. *Anal. Lett.* **2012**, *45*, 1604–1616. [[CrossRef](#)]

**Publisher's Note:** MDPI stays neutral with regard to jurisdictional claims in published maps and institutional affiliations.



© 2020 by the authors. Licensee MDPI, Basel, Switzerland. This article is an open access article distributed under the terms and conditions of the Creative Commons Attribution (CC BY) license (<http://creativecommons.org/licenses/by/4.0/>).